Boron adsorption kinetics of microcrystalline cellulose and polymer resin

Parth Raval, Neethu Thomas, Lama Hamdouna, Laurent Delevoye, Olivier Lafon, G. Manjunatha Reddy

Boron adsorption kinetics of microcrystalline cellulose and polymer resin

Parth Raval, Neethu Thomas, Lama Hamdouna, Laurent Delevoye, Olivier Lafon, and G. N. Manjunatha Reddy*

University of Lille, CNRS, Centrale Lille, Université d'Artois, UMR 8181−UCCS− Unité de Catalyse et Chimie du Solide, F-59000, Lille, France

*corresponding author: gnm.reddy@univ-lille.fr

Keywords: boron capture, chelate complexes, biomass valorization, solid-state NMR spectroscopy

TOC graphic

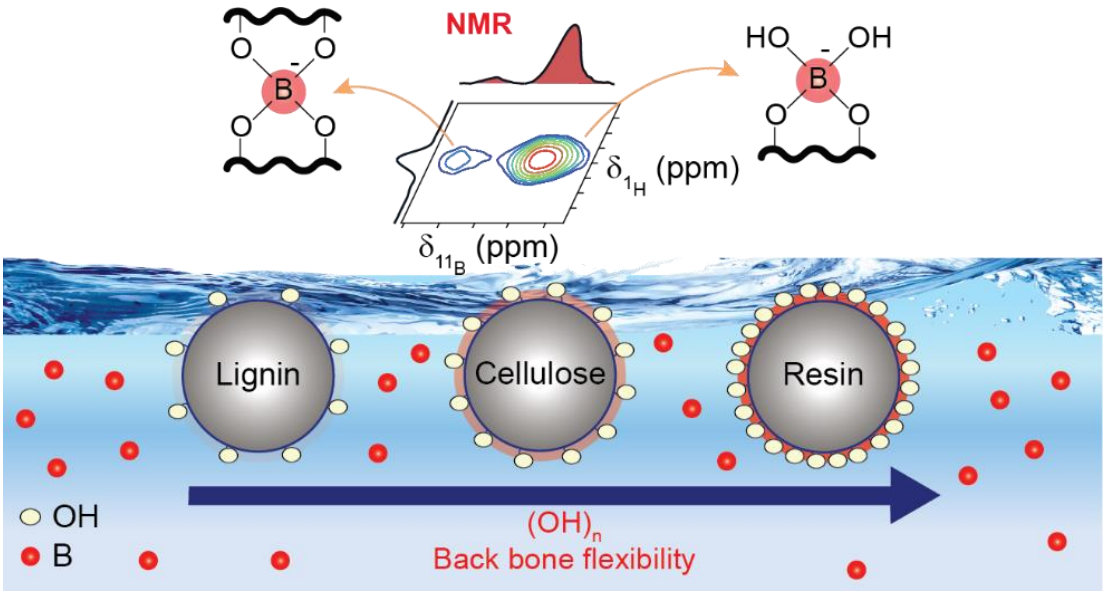

Abstract

Tailoring boron-polysaccharide interactions is an important strategy for developing functional soft materials such as hydrogels, fire retardants and sorbents for environmental remediation, for example, using lignocellulosic biomass. For such applications to be realized, understanding the adsorption kinetics of borate anions on cellulose and their local structures is paramount. Here, the kinetics of boron adsorption by microcrystalline cellulose, lignin and polymeric resin are investigated and compared. Borate anions interact with the vicinal diols in the glucopyranoside moieties of cellulose to yield chemisorbed boron chelate complexes. In contrast to cellulose, technical lignin contains fewer *cis*-vicinal diols, and does not tend to form such chelate complexes upon treatment with the aqueous boric acid solution. The formation kinetics and stability of these chelate complexes strongly depend on nanoscale structures as well as reaction conditions such as pH and concentration of the sorbate and sorbent. Specifically, insights into the distinct boron adsorption sites were obtained by solid-state 1D ^{11}B magic-angle spinning NMR and the local structures and intermolecular interactions in the vicinities of boron chelate complexes are elucidated by analyzing 2D ^{13}C-^{1}H and ^{11}B-^{1}H heteronuclear correlation NMR spectra. The total boron adsorption capacity of cellulose is estimated to be in the 1.3-3.0 mg range per gram of sorbent, which is lower than the boron adsorption capacity of a poly-styrene based resin, ~17.2 mg of boron per gram of Amberlite® IRA 743. Our study demonstrates that the local backbone and sidechain flexibility as well as the structures of polyol groups play a significant role in determining the kinetic and thermodynamic stability of chelate complexes, yielding different boron adsorption capabilities of lignocellulosic polymers.

Introduction

The valorization of various biomass feedstocks and biomass-derived polymers has emerged as one of the most viable routes to develop materials for energy, sustainability, health and environment.[1–5] Plant-derived lignocellulose consists of (hemi)cellulose carbohydrate polymers and lignin composites, the compositions and structures of which strongly depend on the type of biomass feedstock. Chemical conversion through pre-treatment and catalytic conversion pathways are sought to obtain valuable chemicals such as biofuels,[6] platform chemicals, and biogas (or syngas).[7] Other biomass valorization routes include the development of bioplastics, pharmaceutical and healthcare materials, functional hydrogels, fabrics, fire retardants, and environmental remediation materials.[8–10] For example, biomass-derived materials have been designed for the removal of pollutants from aqueous solutions, membranes for water filtration and oil cleanup operations.[11–13] Specifically, cellulose derivatives have been used as borate and phosphate adsorbents.[14–16]

Boric acid chemistry plays an important role in developing functional materials derived from lignocellulose polymers.[17–23] In particular, cellulose-borate interactions have been tailored to engineer wood composites, fabrics, textiles, and fire retardants by forming an impenetrable glass coating on the fire-exposed surface.[17–23] The molecular origins of such properties are related to the degree of boron crosslinking in cellulose polymers and the kinetics of boron adsorption, which enhance the mechanical strength of cellulose and facilitate self-healing capacity. As a result, boron-based functionalization of cellulose has been utilized in a wide range of research areas; nanocomposite hydrogels,[24,25] environmental remediation,[12,26,27] and actuators/sensors.[28,29] Owing to its low solubility in water and tendency to interact with borate anions, cellulose can be used as a low-cost sorbent for scalable boron removal technology[30]. Among the boron removal technologies such as reverse osmosis,[31] electrodialysis[32] and electrocoagulation,[33] boron capture

by ion exchange[34–37] is the most efficient approach due to its high adsorption capacity, economic viability and recyclability. Examples of anion exchange resins include Diaion CRB02® and Dowex® (**Figure S1**), which are capable of achieving the total boron adsorption capacity of tens of milligrams of boron per gram of resin.[38,39] Within the recent past, polysaccharides[40] and biopolymers[41,42] such as chemically modified cellulose,[43] chitosan,[44] and lactose-modified chitosan have been employed as a low-cost alternative for boron removal from aqueous solutions.[45,46] For such applications to be realized, a more elaborative understanding of the surface boron adsorption kinetics as well as the borate-carbohydrate intermolecular interactions is required to be systematically analyzed and compared.

The monomeric D-glucose units of cellulose are covalently linked by β(1→4)-glycosidic bonds, whereby all hydrogen atoms are in an axial position, and hydroxyl groups are in an equatorial position. The hydroxyl groups provide the surface and interfacial reactivity, for example, via hydrogen bonding interactions, leading to different degrees of crystallinity, structural and mechanical properties. Due to these inter- and intramolecular interactions and conformational flexibility,[47,48] a substantial amount of cellulose and the cellulose-derived materials exist as amorphous materials – though crystallites of nanocellulose with dimensions of ~5 nm have been reported [49] – making it difficult to characterize these materials by long-range techniques. Nevertheless, X-ray diffraction (XRD), and Fourier transform (FT) Raman spectroscopy have been employed to gain insight into the degree of order and crystallinity in cellulose.[50] As a local probe, solid-state (ss)NMR spectroscopy has previously been applied to gain insight into the local structures of cellulose and cellulose-lignin interactions in neat cellulose and biomass-derived lignocellulose compounds.[51–60] Within the recent past, surface-enhanced dynamic nuclear polarization (DNP) NMR spectroscopy has been used to characterize functional groups on the

surface of cellulose fibers in paper materials,[56] drug-functionalized TEMPO-oxidized cellulose nanofibrils,[58] and cellulose ethers.[60]

Here, we investigate the kinetics of boron adsorption in cellulose, lignin and polymeric resin material (Amberlite® IRA-743) are studied and compared. The local structures of different boron adsorption sites and the intermolecular interactions between borate anions and cellulose polymers are characterized by 1D ^{11}B MAS and 2D ^{1}H-^{11}B correlation NMR spectroscopy. 1D ^{11}B MAS NMR of boron-adsorbed cellulose provides information on the surface boron adsorption kinetics, chelate complex formation and provides an estimate of the boron adsorption capacity of cellulose. The roles of external factors such as sorbate and sorbent concentration, and pH of the solution on the boron adsorption capacity are examined. SSNMR results are correlated and complemented with FTIR spectroscopy. The impact of boron uptake on the local structures and conformations of the cellulose is investigated by 2D ^{13}C-^{1}H and ^{11}B-^{1}H heteronuclear correlation NMR experiments. These results indicate that the cellulose exhibits a greater tendency towards boron adsorption at basic (pH = 11 or greater) conditions, due to the formation of kinetically stable *bis*-chelate complexes than the labile *mono*-chelate complexes.[40, 69, 70, 71] The cellulose fibers adsorb in the range of 1.3 to 3.0 mg of boron per gram of sorbate depending on the concentration of the sorbent, but the polymeric resin Amberlite® IRA-743 can uptake up to 17.2 mg of boron per gram of resin. A detailed ssNMR study of these materials provides a molecular level understanding of borate-sorbate interactions and the boron adsorption kinetics functionalized by polyol moieties, while unraveling the vital role of the backbone structures, molecular confirmation, and the densities of polyol groups in the total boron adsorption properties of cellulose fibers, thus demonstrating the potential for developing inexpensive and environmentally friendly alternatives for boron capture.

Experimental Methods

Materials and sample preparation. Cellulose (20 μm), Amberlite® IRA743, lignin, NaOH, and boric acid were obtained from Sigma Aldrich (analytical grade) and used as received. To understand the role of external stimuli on the boron adsorption properties of lignin and cellulose, boron uptake reactions were carried out under different conditions (i) by varying the boric acid concentration in aqueous solution and (ii) by modifying the pH of the solution. In the first case, vials containing 80 mg of cellulose were treated with 1 ml of aqueous solutions containing 5.8, 11.6, 22.7, 33.8, 67.2, and 134.2 g/L of boric acid. This concentration range (5.8 - 134.2 g/L) was chosen based on the theoretical maximum boron chelation obtained when all hydroxyl groups in cellulose structure are involved. The pH of these aqueous solutions was maintained constant at ~11 by adding 1 M NaOH solution and progressively monitoring the basicity using a pH meter. In the second case, vials containing 80 mg of cellulose were treated with 1 ml of 33.5 g/L boric acid solutions, whereby the pH values were adjusted to 5, 7, 9, 11 and 13 by adding 0, 4, 120, 460, and 650 μL of 5 M NaOH, respectively. All vials were subjected to vortex agitation for 5 minutes, and the resulting milky-white solutions were allowed to be set at room temperature overnight. Followed by this, centrifugation (12000 rpm) was carried out for 10 min, and the supernatants were pipetted out. The boron-adsorbed cellulose pellets (solid residue) were extracted, placed in a petri dish, and dried in the hot air oven (72 °C) overnight. The dried samples were collected and stored for characterization by various solid-state NMR spectroscopy methods. Amberlite® IRA743 was used as a control material for the quantification of adsorbed boron by cellulose. For the vials containing 80 mg of Amberlite® IRA-743 resins each, boric acid solution (1 mL) with different concentrations of 5.8, 11.6, 22.8, 33.8, 67.3, and 134.8 g/L was added. The pH of the solutions was maintained at 11, consistently with the boron adsorption conditions used for the cellulose. The

resultant precipitate was soaked overnight, then centrifuged (12000 rpm), and the precipitate was collected and dried at 72 °C.

Solid-state NMR spectroscopy. To distinguish between the different boron adsorption sites and to elucidate the local structures of chemisorbed chelate complexes, multinuclear (^{1}H, ^{13}C, and ^{11}B) 1D and 2D MAS NMR experiments were performed. All spectra were acquired at room temperature on a 9.4 T Bruker Avance Neo NMR spectrometer (Larmor frequencies were ^{1}H = 400 MHz, ^{23}Na = 159 MHz, ^{11}B = 128 MHz, and ^{13}C = 100 MHz, respectively) using a double-resonance 4 mm H-X MAS probehead. In each case, 50 mg of the solid material was packed into a 4 mm (outer diameter) zirconia rotor and fitted with Kel-F® caps. 1D ^{11}B NMR spectra were acquired at 8 kHz MAS using high power decoupling (SPINAL-64) pulse sequence for proton decoupling.[62] All 1D ^{11}B MAS NMR spectra were acquired with a dedicated 4 mm H-X probehead to eliminate the strong boron background signal (i.e., boron-free). The nutation frequency was 100 kHz corresponding to a 90-degree pulse length of 2.5 µs. The 1D spectra result from averaging 512 transients with a recycle delay of 5 s, corresponding to a total experimental time of 43 min. The ^{11}B shifts were calibrated using sodium borohydride ($NaBH_4$) as an external reference (^{11}B shift at −42.06 ppm).[63] 1D ^{23}Na MAS NMR spectrum of boric acid-treated cellulose was acquired using 160 co-added transients using single-pulse experiment with 8 kHz MAS frequency, whereby 90-degree pulse duration was 3 µs and the recycle delay was set to 3s. To elucidate the local structures of boron chelate complexes, cross-polarization (CP) based 2D ^{11}B-^{1}H heteronuclear correlation (HETCOR) NMR spectra of the cellulose-borate sample were acquired and analyzed. The nutation frequencies of ^{1}H and ^{11}B were 100 kHz and 84.5 kHz. The 2D ^{11}B-^{1}H HETCOR spectrum was acquired with a CP contact time of 1 ms, and a high-power decoupling (DUMBO) pulse sequence was applied in the indirect ^{1}H dimension.[64] The spectra were acquired with 128 t_1 increments in the indirect dimension, and 16 transients were co-added with a recycle delay of 3 s.

To further corroborate these experiments, solid-state ^{1}H-detected cross-polarization (CP) based ^{1}H-^{13}C heteronuclear correlation (HETCOR) NMR spectra of cellulose-borate and neat cellulose were acquired and compared.[65] These spectra were acquired at 18.8 T Bruker Avance Neo NMR spectrometer at a spinning frequency of 50 kHz using a double-resonance H-X 1.3 mm MAS probehead. 2D ^{1}H-^{13}C HETCOR spectra were recorded with 128 t_1 increments in the indirect dimension, each by co-adding 128 and 96 scans for cellulose-borate and neat cellulose, respectively, with a recycling delay of 5 s.

For boron adsorbed polymeric resin (Amberlite® IRA743), all 1D and 2D MAS NMR spectra were acquired at 18.8 T Bruker Avance Neo NMR spectrometer (Larmor frequencies of ^{1}H = 800.1 MHz, ^{11}B = 257 MHz and ^{13}C = 201 MHz) with 50 kHz MAS using a double-resonance H-X 1.3 mm MAS probehead. 1D ^{1}H MAS spectra were acquired with 100 kHz r.f. pulses by co-adding 16 transients with an interscan delay of 4 s. 1D ^{11}B MAS spectra were acquired with 320 co-added transients with an interscan delay of 3s. Similar acquisition was carried out with an empty rotor under identical experimental conditions, in order to suppress the background peak by subtracting this signal with the ^{11}B MAS spectrum of the boron adsorbed resin. For 1D ^{13}C{^{1}H} CP-MAS spectra, 2048 co-added transients were acquired with 0.2 ms and 4 ms of CP contact times. Solid-state ^{1}H-detected cross-polarization based ^{1}H-^{13}C heteronuclear correlation (HETCOR) NMR spectra of boron adsorbed Amberlite® IRA743 spectra were recorded with 106.4 kHz and 162.3 kHz nutation frequencies of ^{1}H and ^{13}C, respectively. The 2D ^{1}H-^{13}C CP-HETCOR NMR spectrum was acquired with a CP contact time of 4 ms, using 180 t_1 increments in the indirect dimension, each with 64 transients using a recycle delay of 3 s. For 2D ^{11}B-^{1}H CP-HETCOR NMR spectra were acquired with 1 ms and 4 ms of CP contact times. The indirect dimension was acquired by adding 56 t_1 increments, each with 64 transients using an interscan delay of 3 s. The 2D ^{1}H-^{1}H double-quantum (DQ) single-quantum (SQ) spectra were acquired using the Back-to-Back (BaBa)

sequence with one rotor period. For the indirect DQ dimension, 115 t_1 increments were acquired, each by co-adding 16 transients, using States method to achieve sign discrimination.

Since boron-treated lignin does not precipitate, we carried out ^{11}B liquid state NMR experiments on lignin suspended in a pH-controlled boric acid solution. Approximately 40 μL of the liquid sample was packed into a 4mm zirconia rotor and closed with a plastic lid and Kel-F® drive cap. The ^{11}B NMR spectra were acquired with the same experimental parameters used for cellulose but under static conditions.

Attenuated total reflectance Fourier transform infrared (ATR-FTIR) spectroscopy. Perkin Elmer FTIR Spectrum two UATR spectrometer was used to acquire IR spectra of neat and boric-acid treated cellulose powders. The spectra were acquired with 10 scans with a spectral resolution of 0.5 cm^{-1}.

Results and discussion

Upon addition of boric acid solution to lignin, no precipitate was observed for a wide range of boric acid concentrations (5.8-33.8 g/L) and pH values (7.0- 11.0). Therefore, the lignin suspension in boric acid solution was investigated by liquid-state ^{11}B NMR experiments. These results are presented in supporting information (**Figure S2).** In comparison, cellulose is insoluble in water, and only sparingly soluble in a buffer solution, leading to the precipitation of borate-sorbent complexes, which were filtered, dried, and characterized using solid-state FT-IR and NMR spectroscopy techniques (*vide infra*). The boron adsorption kinetics of cellulose and polymer resin Amberlite® IRA743 were separately studied and compared, as discussed below.

Distinct boron binding sites in cellulose. In order to understand the boron adsorption kinetics of cellulose, it is essential to distinguish between different boron adsorption sites and estimate their relative populations. Studies have shown that the borate anion interacts with polyhydroxy groups

by forming chelate complexes.[66–71] The equatorial hydroxyl groups in the glucopyranose ring are open to cross-linking, i.e. interchain dimerization, reactions between the adjacent cellulose or directly coordinate to borate anions to form chelate complexes as shown in the inset of **Figure 1**. Solid-state ATR-FTIR spectra of neat and boric acid-treated cellulose show identical vibrational frequencies (**Figure S3**). Next, we applied ssNMR spectroscopy to analyze distinct boron adsorption sites on cellulose polymers. Owing to its high natural abundance (80.1%) and moderate-to-low quadrupolar coupling constants (0.2 MHz ≤ C_Q ≤ 2.5 MHz), ^{11}B NMR is a sensible probe to detect the chelate complexes of cellulose. Specifically, the isotropic chemical shifts (δ_{iso}) and C_Q values of the ^{11}B sites provide insight into the coordination geometry around boron atoms.[72] It has been shown that tetra-coordinated boron atoms exhibit narrow peaks due to low quadrupolar coupling interactions and highly symmetric chemical bonding environments, as compared to tri-coordinated boron atoms.

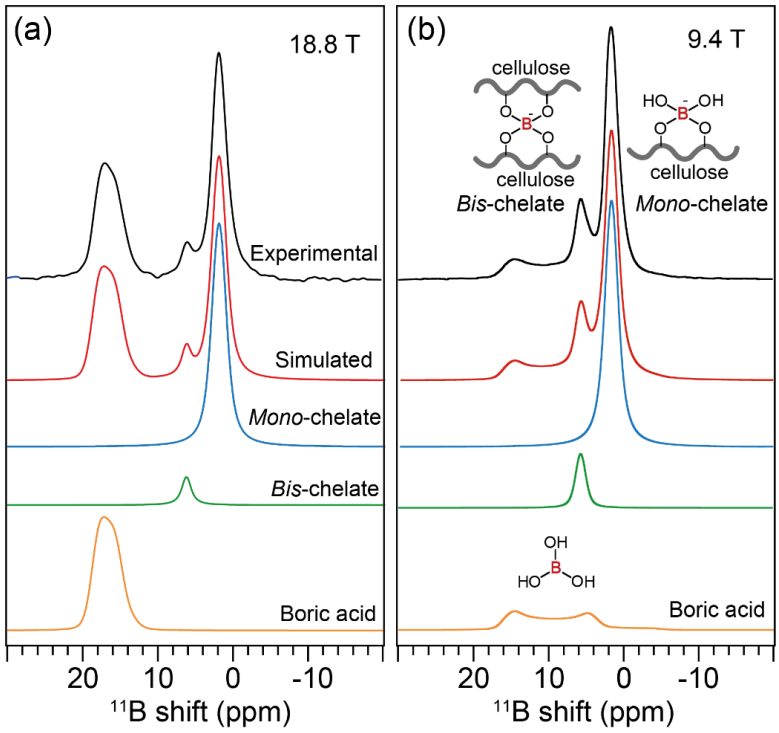

Figure 1. Solid-state 1D (a) ^{11}B MAS NMR spectra of boron adsorbed cellulose acquired at (a) 18.8 T (50 kHz MAS using a Hahn echo sequence) indicating the distinct boron adsorption sites

and (b) at 9.4 T (8 kHz MAS with a single-pulse sequence with high power ^{1}H decoupling) together with deconvoluted analysis of chelate complexes and free boric acid.

Figure 1 presents 1D ^{11}B MAS NMR spectra of boron-adsorbed and dried cellulose powder acquired at (a) 18.8 T (50 kHz MAS) and (b) 9.4 T (8 kHz MAS with ^{1}H-decoupling). The protocol used for the boron adsorption is presented in the experimental details. In addition, the ^{11}B MAS spectra acquired at 18.8 T with different MAS frequencies together with the full spinning sideband patterns are presented in SI (**Figure S4**). This material exhibits well-resolved ^{11}B signals at 1.9 and 6.0 ppm, which are attributed to distinct boron adsorption sites. Based on the ^{11}B signal assignments of tetrahedrally coordinated borate anions in chelate complexes presented in the literature,[66,71] the ^{11}B intensities at 1.9 ppm and 6 ppm are attributed to the different boron chelate (most likely *mono*- and *bis*-chelate) complexes, which will be further corroborated by analyzing 2D correlation NMR spectra (*vide infra*). The ^{11}B peak at ~18 ppm is due to tri-coordinated boron atoms in the unreacted boric acid.[73] Specifically, the high-resolution ^{11}B MAS spectrum obtained at 18.8 T and 50 kHz MAS enabled the different boron signals to be distinguished and identified. For the ^{11}B MAS spectra acquired at 18.8 T and 9.4 T, the lineshape fitting analysis is carried out in order to deconvolute the peaks corresponding to the distinct tri- and tetra-coordinated boron atoms in boron chelate complexes and boric acid components.[72] Using this analysis, the δ_{iso}, C_Q and asymmetry (η_Q) parameters were obtained and compared (**Table 1**). These results suggest that the borate anions are chemisorbed on cellulose in the form of chelate complexes, which are expected to be stabilized by the counter cations such as Na^+ ions that originate from the NaOH used for the regulation of pH. It is further confirmed by acquiring 1D solid-state ^{23}Na NMR spectra of boric-acid-treated cellulose **(Figure S5)**, which exhibit a signal centered at ~5 ppm, indicating the presence of Na^+ species.

Table 1. ^{11}B best-fit NMR parameters, δ_{iso}, C_Q, and η_Q of distinct boron sites in cellulose treated with 33.8 gL^{-1} boric acid at pH = 11.

	Boron species	δ_{iso} (ppm)	C_Q (MHz)	η_Q
18.8 T	*Mono*-chelate	1.8	0.3	0.01
	Bis-chelate	6.1	0.4	0.02
	Unreacted boric acid	19.1	2.5	0.10
9.4 T	*Mono*-chelate	1.9	0.4	0.01
	Bis-chelate	6.0	0.4	0.01
	Unreacted boric acid	18.6	2.4	0.13

[a] Errors on the δ_{iso}, $C_{Q,}$ and η_Q are estimated as ±0.1 ppm, 0.1 MHz, and 0.01, respectively.

Next, we analyzed the boron adsorption kinetics by means of chelate complexes on carbohydrate polymer surfaces/interfaces as a function of boric acid concentration between 5.8 and 134.2 g.L^{-1}. This concentration range is chosen based on the theoretical maximum that postulates all the hydroxyl groups in the cellulose are available and involved in the formation of boron chelate complexes. **Figure 2a** compares the ^{11}B{^{1}H} MAS NMR spectra of boric acid treated cellulose acquired at 9.4 T using a dedicated 4 mm H-X probehead to eliminate the background ^{11}B signal, whereby an increase in the peak intensities at 1.9 ppm and 5.9 ppm as a function of increasing boric acid concentration is evidenced. It is noteworthy that the kinetically stable *mono*-chelate complexes are formed at much faster rate than the thermodynamically stable *bis*-chelate complexes. To test this, we carried out ^{11}B{^{1}H} cross-polarization (CP) MAS NMR

spectra of boron adsorbed cellulose powder with different CP contact times in the range of 0.2 ms to 8 ms, and the CP intensity build as a function of contact time is plotted and compared for the different chelate complexes (**SI, Figure S6)**. Both *mono*- and *bis*-chelate complexes exhibited maximum CP intensity at 1-2 ms of contact time. Due to the presence of labile hydroxyl groups in *mono*-chelate complexes, they are open to exchange reactions when the boron adsorbed cellulose is dissolved in water and buffer solutions with other metal cations (Na^+ ions used for adjusting the pH), as will be further confirmed by subsequently washing the boron adsorbed cellulose material with Millipore water (*vide infra*). The bis-chelate complexes are formed by covalently cross-linking two cellulose fibrils, thus expected to be thermodynamically more stable. The relative populations of these two complexes (**Figure 2b**) strongly depends on the pH dependent speciation of borate anions and boric acid moieties, as discussed below (*vide infra*). However, the signal corresponding to boric acid (5-15 ppm, due to large quadrupolar interaction) was observed at 18.6 ppm, the intensity of which increased as the boric acid concentration increased. It indicates that there exists some degree of unreacted boric acid when the material is treated with excess of boric acid (20 g/L or higher) due to the saturation of boron adsorption sites on the cellulose sorbent. To further confirm that the *mono*-chelate complexes are open to exchange reactions and boric acid is phase separated and does not involve in the formation of chelate complexes, we subsequently washed the resin samples. For the dried powders of boron adsorbed cellulose obtained before and after washing with water, the ^{11}B MAS NMR spectra were acquired and compared **(SI, Figure S7)**. For the rinsed, washed and dried boron adsorbed cellulose, ^{11}B peak intensities associated with the *mono*-chelate and boric acid are substantially reduced, however, the ^{11}B peak of the *bis*-chelate complex is largely retained. These results confirm that the unreacted boric acid and the labile *mono*-chelate complexes are open to exchange reactions, which are washed away during this process, allowing the more stable *bis*-chelate complexes to be retained on the cellulose.

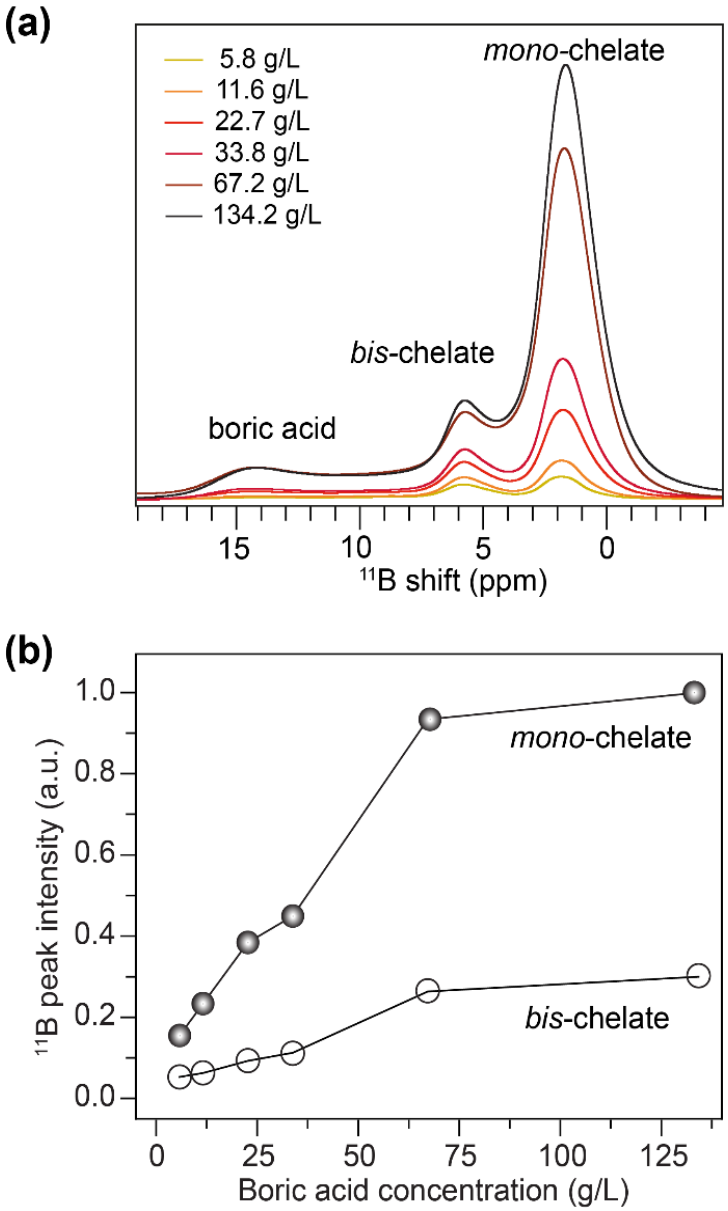

Figure 2. Boron adsorption kinetics of borate *mono*- and *bis*-chelate complexes on microcrystalline cellulose at pH = 11. (a) solid-state 1D $^{11}B\{^{1}H\}$ MAS NMR spectra plotted as a function of boric acid concentration. Peaks corresponding to *mono*- and *bis*-chelate complexes and boric acid are depicted. (c) ^{11}B peak intensity of *mono*- and *bis*-chelate complexes to the plotted as a function of boric acid concentration.

The δ_{iso}, C_Q, and η_Q values of the ^{11}B signals associated with the boron chelate and boric acid sites did not change substantially (**Table 1** and **SI Table S1**), as function of increased boric acid

concentration. Subtle changes in the C_Q values between 2.1 and 2.4 MHz for the boric acid signal is within the error bars (± 0.1 MHz). These values are consistent with tri and tetra-coordinating boron sites reported in the previous studies.[72,74,75] However, the tendency of forming *bis*-chelate complexes is reduced with the increasing boric acid concentration, and the formation of *mono*-chelate complexes is more favored (**Figure 2**). This is because the formation of *bis*-chelate complexes requires two cellulose units along the polymeric cellulose chain (or between the adjacent polymer chains) to be cross-linked, which is sterically more demanding than the mono-chelate complexes that can adsorb on the same cellulose monomer. At dilute concentrations of borate anions, ≤ 15 g/L, both of these sites are accessible for the chemisorption of borate anions. When the concentration of boric acid is > 15 g/L, *mono*-chelate complexes are sterically more accessible than the *bis*-chelate complexes. In contrast to this, synthetic polymer resins such as Amberlite® IRA743 designed for boron adsorption take into account these structural factors to enhance the boron uptake, whereby the flexible surface-functionalized polyhydroxy groups (*cis* diols) attached to the polymer backbone favor the formation of *bis*-chelate complexes, which are thermodynamically more stable than the *mono*-chelate complexes.[66] As such, the natural cellulose structure lacks *cis*-diols, which limits its tendency to form a *bis*-chelate complex. In addition, the role played by the concentration of borate anions ($B(OH)_4^-$) over the boric acid (H_3BO_3) in the formation of these complexes cannot be merely ignored.

Impact of pH-dependent boric acid speciation on boron adsorption kinetics. Having analyzed the role of boric acid concentration, we then examined the impact of pH on the total boron adsorption properties of cellulose. In an aqueous solution, boric acid act as a Lewis acid , forming a Lewis acid base adduct $[B(OH)_4]^-$ with hydroxyl groups as depicted in **Equation 1**.

$$H_3BO_3 + H_2O \rightleftarrows B(OH)_4^- + H^+ \qquad 1$$

Due to the weak Lewis acidity of boric acid, the boron speciation in the form of boric acid and borate anions in an aqueous medium depends strongly on the pH.[39] The acid dissociation constant (pK_a) of boric acid was found to be ~9.14, i.e., at pH = 9.14, the boric acid and borate anion are in equilibrium. At a pH greater than 9.14, the tetrahedral borate anion $[B(OH)_4]^-$ dominates, while at a pH lower than 9.14, trigonal boric acid $B(OH)_3$ predominates. However, it has been shown that borate anions are preferred over boric acid in order to interact with diols.[74] It prompted us to study the boron adsorption by cellulose as a function of pH.

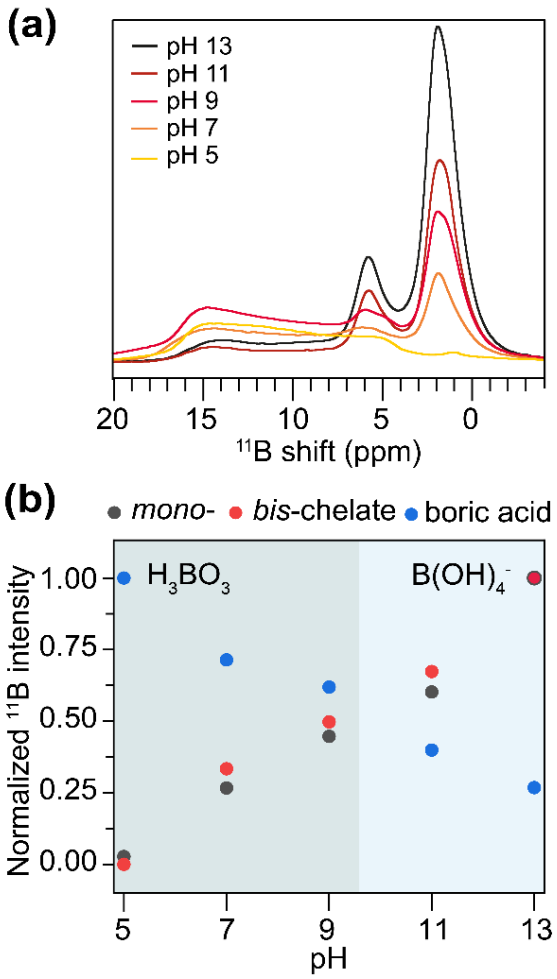

Figure 3. (a) Solid-state 1D $^{11}B\{^1H\}$ MAS NMR spectra of cellulose treated with boric acid at different pH values, as indicated in the inset. (b) A plot of normalized intensities of boron signals

associated with boric acid and *mono*- and *bis*-chelate complexes as a function of pH. The green and blue-shaded areas represent the pH where boric acid and borate anions predominantly exist, respectively. All spectra were acquired at 9.4 T (8 kHz MAS and 298 K) under identical conditions.

Figure 3a compares the 1D ^{11}B MAS NMR spectra of 33.5 g.L^{-1} boric acid-treated cellulose as a function of pH. The pH was adjusted by progressively adding NaOH solution dropwise to the cellulose borate solution until the target pH was reached, as monitored by a pH meter. The boric acid concentration of 33.5 g.L^{-1} in water gives rise to a pH of ~5.4, at which signals corresponding to the chelate complexes are barely detected. At pH = 7, the ^{11}B signal (1.9 ppm) associated with the *mono*-chelate complex becomes evident, and its intensity increases as the pH value increase up to 13. A similar trend is observed for the ^{11}B signal of the *bis*-chelate (5.9 ppm) complex. The ^{11}B peaks of *mono*-chelate and the *bis*-chelate complexes have reached a maximum intensity at pH = 13. This could be due to deprotonation of hydroxyl groups in aqueous alkali[76] and the highly abundant borate anion at alkaline pH, allowing it to interact with diols of cellulose. In contrast to the boron atoms in chemisorbed chelate complexes, the ^{11}B signal intensity of the free boric acid decreases at a relatively higher pH, i.e., a more alkaline medium, because the equilibrium shifts towards borate anion, which facilitates the formation of chelate complexes. **Figure 3b** presents the normalized intensities of boron signals (obtained by comparing the intensity of each peak with respect to the most intense peak for the particular site) associated with boric acid and *mono*- and *bis*-chelate complexes plotted as a function of pH. It shows a monotonic increase in the adsorbed boron on the cellulose surface by means of *mono*- and *bis*-chelate complexes, and simultaneously, the amount of free boric acid decreases as a function of increasing pH, consistently with the dissociation of boric acid (**Equation 1).** For the different ^{11}B signals shown in **Figure 3a**, the quadrupolar fitting parameters are listed in **Table S2.** The quadrupolar coupling constants (C_Q) for *mono*-chelate and *bis*-chelate signals vary from 0.8 MHz (pH 5) to 0.3 MHz (pH 13) but remain

within 1 MHz. As shown in the ^{11}B spectra plotted as a function of boric acid concentration, the free boric acid signal with δ_{iso} = 18.6 ppm exhibits a quadrupolar coupling constant (C_Q) ~2.4 MHz for different pH values. This analysis suggests that the total boron adsorption capacity of cellulose depends on the pH and boric acid concentration in an aqueous solution. During the centrifugation process, the mass of boron adsorbed on cellulose and the mass of boron leached into the supernatant solution were estimated and compared for the different boric acid concentrations. These results are presented in SI (**Table S3**).

Structure elucidation of boron chelate complexes. Although 1D ^{11}B MAS NMR experiment enabled tri- and tetra-coordinated boron sites to be distinguished, it does not provide information on the local structures of *mono*- and *bis*-chelate complexes. In addition, 1D ^{13}C and ^{1}H MAS NMR spectra of cellulose before and after exposure to boron (**Figures S8-S10** and **4a**) exhibit severely overlapping resonances even for the spectra acquired at 18.8 T, which makes it difficult to probe the subtle displacements in the frequencies and peak intensities. To elucidate the local structures of borate-cellulose chelate complexes, we separately carried out 2D ^{1}H-^{13}C and ^{11}B-^{1}H cross-polarization based heteronuclear correlation (HETCOR) NMR experiments, which resolve the ^{1}H, ^{13}C, and ^{11}B peaks based on the through-space dipolar-coupled ^{1}H-^{11}B and ^{1}H-^{13}C sites. The line-cut row or column ^{1}H-spectra at specific ^{13}C and ^{11}B chemical shifts are presented in SI (**Figure S10**). In the 2D ^{1}H-^{13}C HETCOR spectrum (**Figure 4a**), the ^{13}C peaks in the vertical axis at 104.8, 83–98.3, 68–78.4, and 62–64.8 ppm are attributed to the carbon atoms on the glucose ring at C1, C4, C2, 3, 5, and C6, respectively,[77,78] and a broad ^{1}H peak at 3.4-4.6 ppm on the top horizontal axis is due to the different proton sites in the pyranose ring, the ^{1}H peak assignment was further aided by the 2D ^{1}H-^{13}C HETCOR spectrum. The ^{1}H and ^{13}C chemical shifts corresponding to the ^{1}H-^{13}C proximities in the cellulose framework are listed in **Table 2**, whereby the C1 at 104.8 ppm

was correlated with H1 at 4.6 ppm. The C6 at 64.4 ppm was correlated with H6 signals at 3.7 and 4.2 ppm and OH signal at 4.7 ppm. The C4 and C4′ signals at 81.7 and 88.3 ppm, originating from the amorphous and crystalline regions, were correlated with H4 signals at 3.4 and 3.5 ppm, respectively. The broad feature at 68-77 ppm (^{13}C) is due to overlapping cross-peaks from C2, C3, and C5 sites, and the proton peaks correlated to these carbon atoms are poorly resolved in the 2D ^{1}H-^{13}C spectra. These results are complemented by analyzing the 2D ^{11}B-^{1}H HETCOR spectrum, which further improved the resolution capability by detecting the 2D ^{11}B-^{1}H peaks for the proton sites dipolar coupled with boron atoms in the vicinity of borate-cellulose chelate complexes (**Figure 4b).** Specifically, the ^{11}B signal at 1.9 ppm correlated to H6 at 3.7 ppm and was assigned to the *mono*-chelate complexes, and the ^{11}B signal at 5.9 ppm correlated to H6 at 3.7 ppm was assigned to the *bis*-chelate complexes, as shown in **Figure 4b**. Together, the observation of 2D correlation signals in **Figures 4a and 4b** indicates through-space proximities between boron atoms in the chelate complexes and the proton atoms in the cellulose polymers.

Table 2. 2D peaks correlating ^{1}H, ^{13}C, and ^{11}B shifts, originating from ^{1}H-^{13}C proximities and ^{1}H-^{11}B proximities in the boron-treated cellulose

^{1}H-^{13}C sites	^{1}H-^{11}B sites	^{1}H chemical shift (ppm)	^{13}C chemical shift (ppm)	^{11}B shift (ppm)
C1-H1	-	4.6	104.8	-
C4-H4	-	3.4	81.7	-
		3.5	88.3	
C6-OH	-	4.7	64.4	-
C6-H6	B-H6	4.2	64.4	5.9
		3.7	64.4	1.9

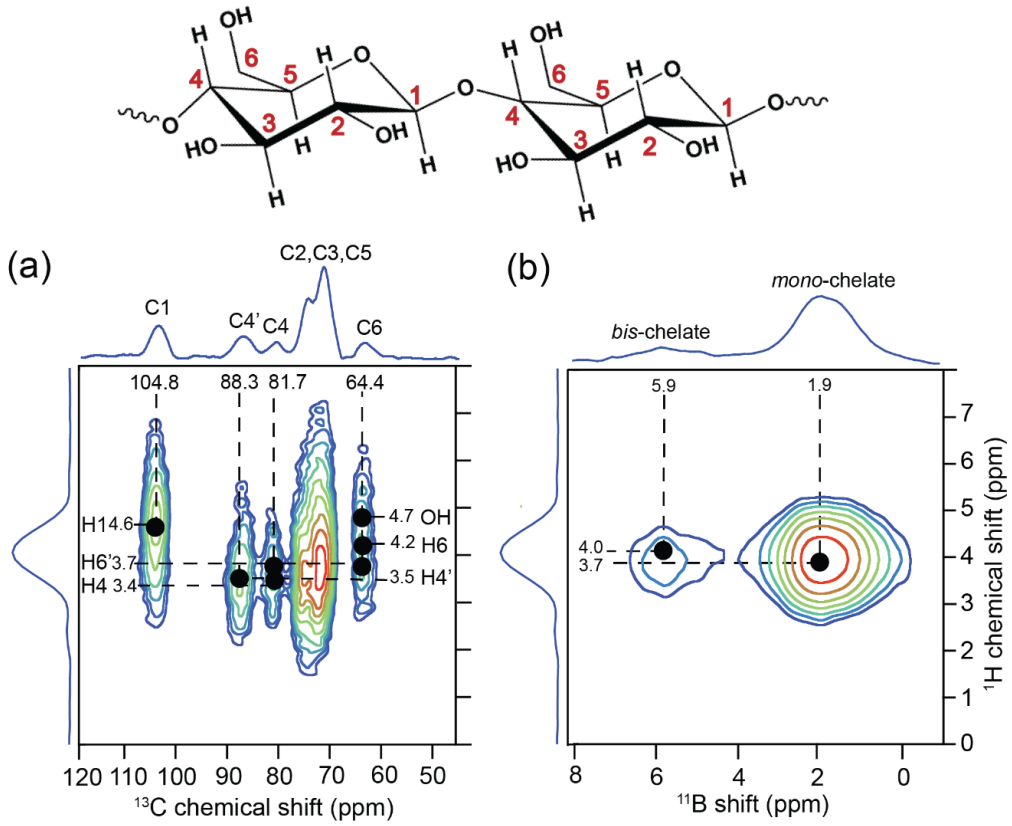

Figure 4. (a) Solid-state 2D ^{1}H-^{13}C HETCOR NMR spectrum (18.8 T and 50 kHz MAS) of boric-acid treated cellulose using a CP contact time of 2 ms. (b) Solid-state 2D ^{11}B-^{1}H heteronuclear correlation NMR spectrum (9.4 T and 8 kHz MAS) of boric-acid treated cellulose were acquired using a CP contact time of 1 ms. The 2D ^{1}H-^{13}C spectrum is tilted by 90 degrees to compare the ^{1}H chemical shifts on the vertical axis. Dashed lines depict the assignments of 2D ^{1}H-^{11}B and ^{1}H-^{13}C correlation peaks to the corresponding ^{1}H and ^{13}C sites indicated in the schematic structure (top).

Boron adsorption capacities of lignin, cellulose, and Amberlite® IRA743. To understand the role of backbone structures and polyol groups on the total boron adsorption capacity, we studied and compared the boron adsorption properties of structurally different polymers such as cellulose, lignin, and synthetic resin. A key limitation associated with technical lignin as a sorbent for boron capture is due to the structural constraints, including the aromatic rings and the presence of phenolic hydroxyl, aliphatic hydroxyl, benzyl alcohol, noncyclic benzyl ether, carbonyl groups,

and methoxyl groups in lignin, which makes it readily soluble in water.[79] As a result, lignin treated with an aqueous solution of borate anions yields a dark brown solution, and no precipitation occurred. Although the hydroxyl groups present in lignin are expected to interact with borate anions from the aqueous solution, they are open to exchange reactions with counter cations in solution, as depicted in solution-state ^{11}B NMR spectrum of boric acid-treated lignin that did not show the peaks corresponding to the *mono*- and *bis*-chelate complexes. This spectrum is identical to the liquid-state ^{11}B NMR spectrum of neat boric acid at pH =11, further confirming that the lignin exhibits low affinity towards borate anions. It is noteworthy that the signals from bound boron cations may not be visible in this solution-state ^{11}B NMR spectrum due to the fast relaxation properties of quadrupolar nuclei such as ^{11}B. By comparison, cellulose is a potential biomass-derived compound for boron capture from aqueous solutions due to its low solubility in water and ability to form chemisorbed boron chelate complexes. Therefore, the total boron adsorption capacity of cellulose is compared with a synthetic boron-adsorbing resin Amberlite® IRA743, which consists of a polystyrene matrix with surface functionalized N-methyl D-glucamine (NMDG) groups.

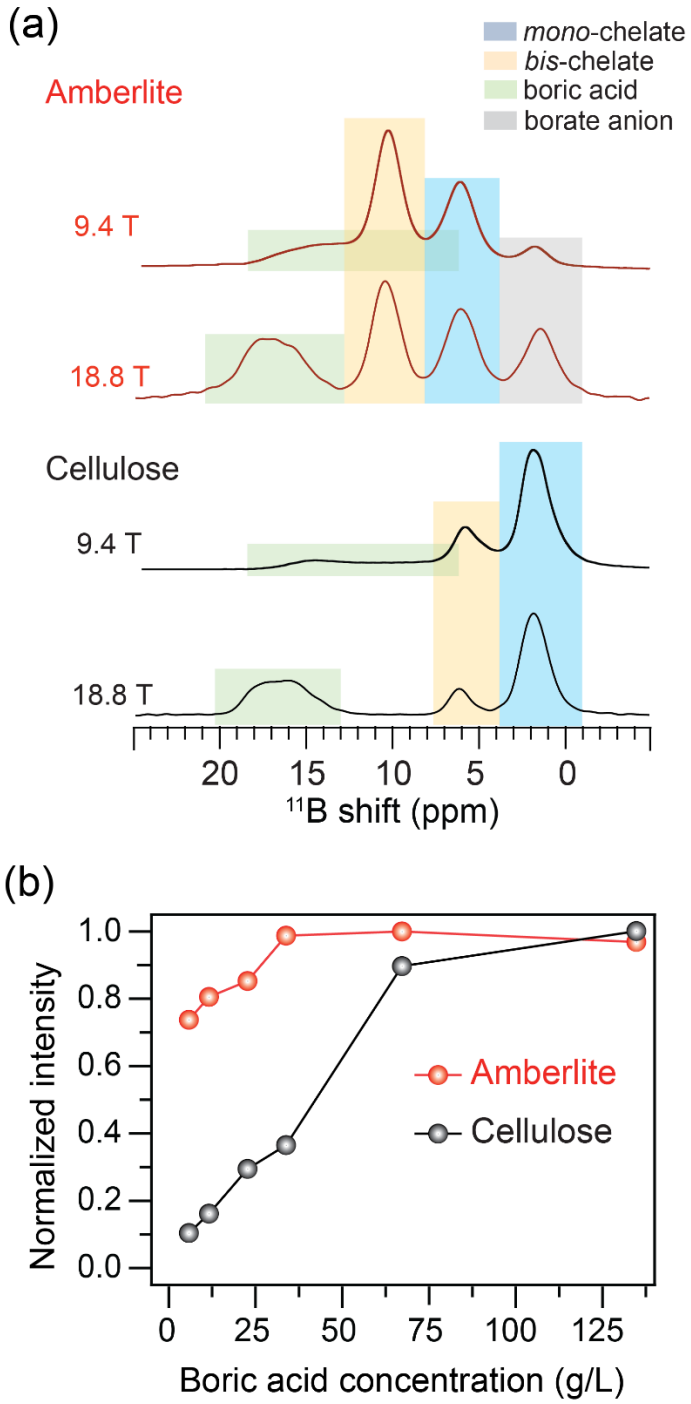

Figure 5. (a) Solid-state 1D ^{11}B NMR spectrum of boron-treated polymeric resin Amberlite® IRA743 (top) and cellulose (bottom) acquired at 9.4 T (8 kHz MAS) and 18.8 T (50 kHz MAS). Resolution enhancement in the ^{11}B MAS spectra acquired at 18.8 T is noteworthy. (b) A plot of normalized ^{11}B intensity of *mono*- and *bis*-chelate complexes combined as a function of boric acid concentration for Amberlite® IRA743 (red dots) and cellulose (black dots). The boric acid concentration used for the boron treatment was 33.8 mg/mL.

In synthetic polymer resin, the high density of hydroxyl groups in NMDG moieties and low solubility of polystyrene backbone are responsible for the enhanced boron uptake. In addition, the amine functional group in Amberlite® IRA743 plays an essential role in the efficient chelating of boric acid by neutralizing the protons released by the formation of chelate complexes, leading to NH_3^+ groups that may also charge balance the borate anions. **Figure 5a** compares ^{11}B MAS spectra of boron-treated (pH = 11) Amberlite® IRA743 and cellulose materials acquired at different magnetic fields. While the spectra acquired at 9.4 T yield to partially overlapped ^{11}B peaks, the well resolved ^{11}B signals obtained in the spectra acquired at 18.8 T enabled the ^{11}B signals corresponding to three distinct boron sites in cellulose and four distinct boron adsorption sites in the polymeric resin to be identified. The enhanced resolution associated with the ^{11}B MAS spectra further enabled the estimation of boron adsorption capacity of these materials, as discussed below. For Amberlite® IRA743, the ^{11}B signal at 10.2 ppm and 6.0 ppm corresponds to *bis*-chelate, and *mono*-chelate complexes,[80] and the signal at 19.0 ppm is due to the free boric acid. Detailed lineshape analysis and their corresponding parameters are presented in **Figure S11** and **Table S4**. In addition, the peak at 2.0 ppm is expected to originate from tetrahedrally coordinated free borate anions with counter cations in the sample.[80] At a controlled pH ~11, the boron uptake of Amberlite® IRA743 increases as the boric acid concentration increases from 5.8 to 134.2 $g.L^{-1}$ **(SI, Figure S12),** similar to that observed for cellulose material.

Figure S13 (SI) presents kinetics of boron adsorption plots by means of normalized intensities of the *mono*-chelate and *bis*-chelate complexes as a function of boric acid concentration (g/L), indicating the different trends in the formation of distinct boron chelating complexes in cellulose and resin. For example, the *bis*-chelate complex is predominantly observed in Amberlite IRA-743 at low boric acid concentrations, whereas the fractions of the *mono*-chelate complex are favored in cellulose. This is due to the different polymeric backbone structures as well as the

densities of polyol groups combined. Therefore, the Amberlite and cellulose materials exhibit different boron-adsorption properties **(Figure 5b)** due to different affinity interactions. As indicated in **Figure 5b,** at low boric acid concentrations (5.0 – 33.8 g/L), cellulose exhibits relatively low boron adsorption than the Amberlite® IRA743, which is intuitive as the structure of Amberlite® IRA743 is particularly engineered to have a strong affinity towards boron species. Upon further increase in the boric acid concentration (greater than 33.8 g/L), the sum of the normalized intensity of the mono-chelate complex and the bis-chelate complex in cellulose increases. Because of this, cellulose and Amberlite® IRA743 exhibit different boron adsorption kinetics. However, both Amberlite® IRA743 and cellulose showed a saturation in the boron adsorption when the boron concentration reached ~65 g/L. Cellulose captures boron by forming less stable *mono*-chelate complexes as major species, whereas Amberlite® IRA743 captures boron by forming stable *bis*-chelate complexes as major species (**Figure S14**). This indicates that the surface-functionalized NMDG hydroxyl groups in Amberlite® IRA743 are key to the enhanced boron adsorption properties. However, understanding the molecular level origins of enhanced boron adsorption by Amberlite® IRA743 necessitates a detailed analysis of local structures of distinct boron adsorption sites.

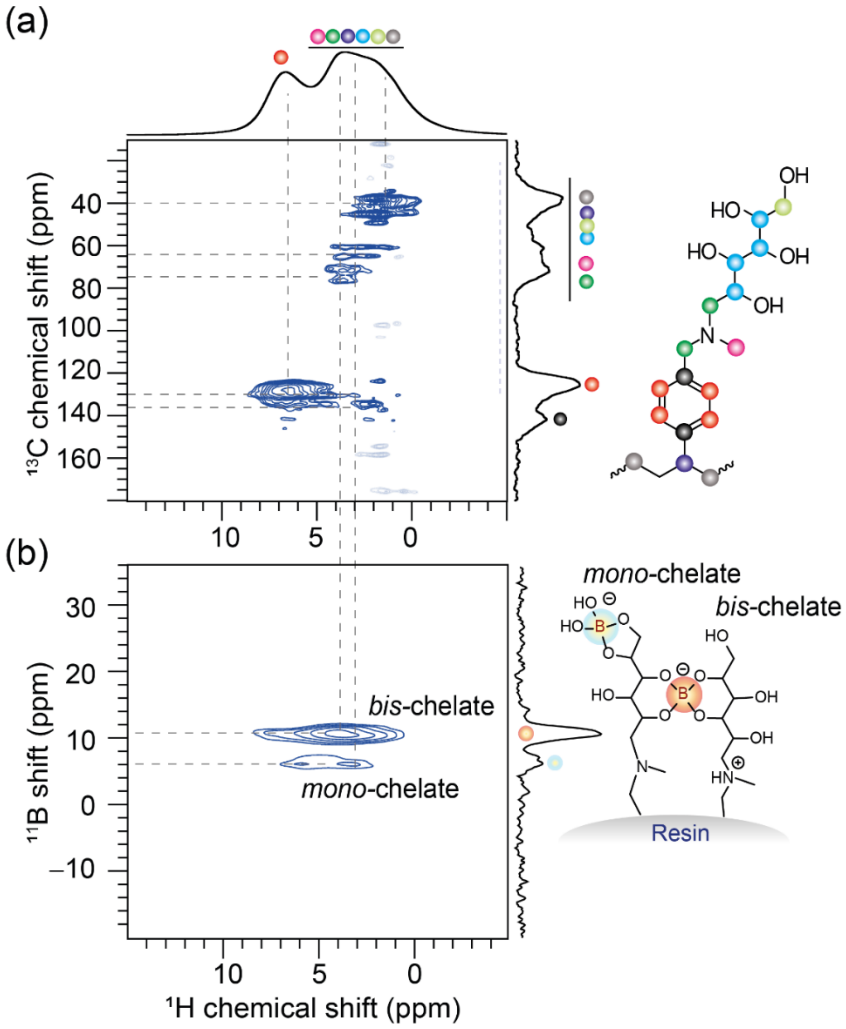

Figure 6. Solid-state (a) 2D ^{1}H-^{13}C (b) 2D ^{11}B-^{1}H heteronuclear correlation NMR spectra of boric-acid treated polymeric resin (amberlite IRA743) acquired with a CP contact time of 4 ms. The 2D ^{11}B-^{1}H spectrum is tilted by 90 degrees to compare the ^{1}H chemical shifts on the vertical axis. Dashed lines depict the assignments of 2D ^{11}B-^{1}H and ^{1}H-^{13}C correlation peaks to the corresponding ^{1}H and ^{13}C sites indicated in the schematic structure (top). All spectra were acquired at 18.8 T with 50 kHz MAS.

To gain insight into the local chemical environments of the different boron adsorption sites in Amberlite® IRA743, we next carried a detailed 1D ^{1}H, ^{13}C, ^{11}B MAS and 2D ^{1}H-^{1}H, ^{11}B-^{1}H, ^{1}H-^{13}C correlation NMR experiments. In the ^{1}H one pulse NMR spectrum (**SI, Figure S15a**) of boron-

adsorbed resin, distribution of peaks in the 1-6 ppm range correspond to the overlapping contribution from the -CH and CH_2, -NCH_3 and -NCH_2 groups of pendant NMDG sidechains. In addition, the broad distribution of peaks centered at 4.5 ppm is attributed to the hydroxyl groups of the surface functionalized NMDG moieties. The broad peak in the 6-7 ppm is due to the aromatic protons associated with the polystyrene divinylbenzene backbone moieties. By comparison, the $^{13}C\{^1H\}$ cross-polarization NMR spectra acquired with the different CP contact times (**SI, Figure S15b**) allowed the directly bonded -CH and the quaternary carbon atoms to be distinguished. In addition, a detailed analysis of 2D ^1H-^1H double-quantum–single-quantum (DQ-SQ) correlation spectrum is presented in **SI (Figure S16),** which provides information on the through-space and dipolar coupled proton pairs in the NMDG groups and the polystyrene divinylbenzene backbones. 2D ^1H-^{13}C correlation experiments provide enhanced resolution, enabling the ^1H peaks corresponding to the different moieties to be identified and analyzed. In the 2D ^{13}C-^1H HETCOR spectrum of boron-adsorbed resin (**Figure 6a**), correlation between ^{13}C signals at 30-50 ppm and ^1H signals at 1-3 ppm are due to the dipole-dipole interactions between protons and carbon atoms the CH_2 moieties of the NMDG groups (pale green dot) and the polymer backbone (gray dots). 2D peaks correlating 54-78 ppm (^{13}C) and 2-4.5 ppm (^1H) indicates the close proximity between carbon and proton sites in the NMDG side chains (green, blue and magenta dots). Specifically, high intensity 2D correlation between ^1H signal around 6-8 ppm and ^{13}C signal in the range of 122-138 ppm is attributed to the ^1H-^{13}C dipole-dipole interactions in the phenyl group of styrene moieties (red dots). Further, the intermediate-range dipole-dipole interactions between carbon atoms of polymer backbone and proton sites of the NMDG sidechains could also be identified by the low intensity correlated intensities of ^{13}C signal centered around 130-138 ppm with ^1H signals at 1-2 ppm and 4-5 ppm range. These results are further corroborated by analyzing the 2D ^{11}B-^1H CP HETCOR spectrum, whereby the through-space and dipolar coupled ^1H and ^{11}B moieties

produce 2D peaks. The most notable of all are the ^{1}H signals associated with the CH and OH sites in the vicinity of *mono*- and *bis*-chelate complexes are resolved and identified. A strong intensity 2D peak correlating ^{1}H (1.7, 3.8 and 7.4 ppm) and ^{11}B (10.2 ppm) shifts is attributed to the formation of *bis*-chelate complexes, which further correlate with the ^{1}H and the ^{13}C chemical shifts in the range of 35-50 ppm and 60-78 ppm that are associated with the -NCH_3, -NCH_2 and CH sites of NMDG groups. This suggests that the hydroxyl groups of NMDG is mainly involved in formation of such complexes. In addition, low intensity correlation peak between ^{1}H (3 and ~5 ppm corresponds to $-CH_2$ and $-NCH_2$ and $-OH$ sites of NMDG moieties) and ^{11}B (6 ppm) chemical shifts are due to the *mono*-chelate complexes. However, there are no 2D correlation peaks associated the boron peaks at 1.5 and ~17.6 ppm in the HETCOR spectra acquired with different CP contact times, further conforming that the free boric acid (~17.6 ppm) and agglomerates of the borate anions (~1.5) ppm are phase separated and boron atoms of which do not exhibit through-space dipolar interactions with the proton sites of the polymeric resin (**SI, Figure S17**). Although the attribution of ^{11}B shift at 10.2 ppm to the formation of amine coordinated borate complexes cannot be completely ignored, the ^{11}B peak at 1.5 ppm does not correspond to the chelate complexes. In addition, comparison of ^{11}B MAS spectrum of the boron adsorbed polymeric resin acquired before and after subsequently washing with Millipore water indicates that the unreacted boric acid species are leached into the solution during the subsequent rinsing and drying process (**SI, Figure S18**). The different ^{11}B shifts associated with the chemisorbed boron sites in cellulose and amberlite are due to the different local bonding environments of boron chelate complexes. These results further confirm that the local chemical environments of the mono- and bis-chelate complexes in the resin are different from the chelate complexes formed by the borate-cellulose interactions. Additionally, this analysis highlights the crucial role of NMDG groups in facilitating boron adsorption by means of *mono*- and *bis*-chelate complexes and leading to enhanced boron

adsorption of polymeric resin. The surface modification and hyperbranching of cellulose by functional groups such as NMDG groups are expected to improve the boron adsorption properties of cellulose materials, owing to the structural/conformational flexibility associated with both pyranose rings and pendent NMDG sidechains.[15,16]

To compare the relative boron-adsorption capacities of cellulose and Amberlite® IRA743, the peak integrals of *mono*- and *bis*-chelate complexes obtained from the deconvolution of 1D ^{11}B NMR spectra of Amberlite® IRA743 were analyzed and compared. A detailed explanation of the estimation of the boron-adsorption capacity is given in **SI (Section 15, Figure S14, Table S5)**. Based on this analysis, the boron-adsorption limit of the cellulose was estimated to be about 1.3-3.0 mg per gram of cellulose, as compared to ~17.2 mg/g in Amberlite® IRA743 resin, when treated with a boric acid solution of concentration of 5.8 g/L at pH = 11. The reason behind employing a 5.8 g/L boric acid concentration is to ensure the minimal presence of free boric acid, and basic pH favors the formation of borate anions. For the materials used in this study, boron adsorption properties of lignin, cellulose, and Amberlite IRA743 are presented in **Tables 3 and S5**. Specifically, cellulose exhibits higher boron uptake than lignin owing to a flexible backbone structure.[47] Besides that, the higher concentration of polyhydroxyl groups is the key factor causing the better boron adsorption in Amberlite® IRA743. Nonetheless, a detailed understanding of cellulose-borate interactions and the related boric acid chemistry are expected to offer far-reaching insights for developing other functional materials, such as cellulose-based hydrogels, remediation, and fire retardants.

Table 3. Boron adsorption capacities of lignin, cellulose, and Amberlite® IRA743.

Polymer	Adsorbed boron (mg) / g of sorbent
Lignin	-
Cellulose	1.3-3.0
Amberlite® IRA-743	17.2

Conclusions

The molecular-level origins of different boron adsorption kinetics in lignocellulose biopolymers, notably, microcrystalline cellulose and lignin are examined and compared with a polymeric resin. Lignin is readily soluble in water and exhibits poor affinity towards boron species. Cellulose-based sorbents are capable of adsorbing borate anions from aqueous solutions. Specifically, 1D ^{11}B MAS NMR spectra acquired at different magnetic fields, 9.4 T and 18.8 T, have been analyzed to identify distinct adsorption sites, i.e., cellulose *mono*-chelate and *bis*-chelate complexes. Quantitative lineshape analysis of the ^{11}B MAS spectra suggests that the boron atoms preferentially form kinetically labile *mono*-chelate complexes over the thermodynamically stable *bis*-chelate complexes. The roles of external stimuli such as boric acid concentration and pH on the boron adsorption kinetics of cellulose are explored by measuring and analyzing ^{11}B NMR spectra, whereby an alkaline condition with a pH greater than 11 is beneficial for boron adsorption. Analysis of 2D ^{1}H-^{13}C and ^{1}H-^{11}B HETCOR spectra of boron-adsorbed cellulose suggest that chemisorbed chelate complexes are in cellulose proximities to the pyranose rings of the cellulose moieties. The boron adsorption capability of cellulose is estimated to be 1.2 mg of boron per gram of sorbent, while Amberlite® IRA743 resin exhibited higher performance due to the presence of

hydroxyl groups in the NMDG groups combined with the backbone and sidechain flexibility of which favors the accessibility towards borate anions to penetrate into the resin surface. Insights into the local structures of different boron chelate complexes in heterogeneous polymeric sorbates are obtained by analyzing 2D correlation NMR spectra. These results reveal that cellulose polymers could seemingly be an option for the removal of boron from aqueous solutions, owing to its low solubility in water, conformational backbone flexibility, and hydroxyl groups. However, surface functionalization of cellulose is required to further enhance the boron adsorption properties. A detailed structural characterization of cellulose-boron interactions further helps to tailor the cellulose-based materials for environmental remediation applications.

Acknowledgements. P.R and N.T contributed equally to this work. This project has received funding from the European Union's Horizon 2020 research and innovation programme under the Marie Skłodowska-Curie grant 79509. SSNMR experiments were carried out at the large-scale NMR facilities co-funded by IR INFRANALYTICS FR-2054.

Supporting Information. Chemical structures, solution-state ^{11}B NMR spectrum of lignin, FTIR spectra of cellulose before and after boron adsorption, solid-state 1D ^{1}H, ^{11}B, ^{13}C and ^{23}Na MAS NMR spectra of boron adsorbed cellulose, 1D ^{1}H, ^{13}C, ^{11}B and 2D ^{1}H-^{1}H, ^{11}B-^{1}H correlation spectra of boron adsorbed resin, and 1D ^{11}B MAS NMR spectra of boron adsorbed sorbates after rinsing and washing, and quantitative analysis of boron adsorption capacities of cellulose and resin.

Conflicts of Interest.

Authors declare no conflicts of interest.

References

(1) Tuck, C. O.; Pérez, E.; Horváth, I. T.; Sheldon, R. A.; Poliakoff, M. Valorization of Biomass: Deriving More Value from Waste. *Science.* **2012**, *337*, 695–699.

(2) Yamakawa, C. K.; Qin, F.; Mussatto, S. I. Advances and Opportunities in Biomass Conversion Technologies and Biorefineries for the Development of a Bio-Based Economy. *Biomass and Bioenergy* **2018**, *119*, 54–60.

(3) Osman, A. I.; Mehta, N.; Elgarahy, A. M.; Al-Hinai, A.; Al-Muhtaseb, A. H.; Rooney, D. W. Conversion of Biomass to Biofuels and Life Cycle Assessment: A Review. *Environ. Chem. Lett.* **2021**, *19*, 4075–4118.

(4) Rahman, M. M.; Liu, R.; Cai, J. Catalytic Fast Pyrolysis of Biomass over Zeolites for High Quality Bio-Oil – A Review. *Fuel Process. Technol.* **2018**, *180*, 32–46.

(5) Briens, C.; Piskorz, J.; Berruti, F. Biomass Valorization for Fuel and Chemicals Production -- A Review. *Int. J. Chem. React. Eng.* **2008**, *6*, 1674.

(6) Appels, L.; Dewil, R. Biomass Valorization to Energy and Value Added Chemicals: The Future of Chemical Industry. *Resour. Conserv. Recycl.* **2012**, *59*, 1–3.

(7) Abraham, A.; Mathew, A. K.; Park, H.; Choi, O.; Sindhu, R.; Parameswaran, B.; Pandey, A.; Park, J. H.; Sang, B. I. Pretreatment Strategies for Enhanced Biogas Production from Lignocellulosic Biomass. *Bioresour. Technol.* **2020**, *301*, 122725.

(8) Das, R.; Lindström, T.; Sharma, P. R.; Chi, K.; Hsiao, B. S. Nanocellulose for Sustainable Water Purification. *Chem. Rev.* **2022**, *122*, 8936–9031.

(9) Ates, B.; Koytepe, S.; Ulu, A.; Gurses, C.; Thakur, V. K. Chemistry, Structures, and Advanced Applications of Nanocomposites from Biorenewable Resources. *Chem. Rev.* **2020**, *120*, 9304–9362.

(10) Okolie, J. A.; Nanda, S.; Dalai, A. K.; Kozinski, J. A. Chemistry and Specialty Industrial

Applications of Lignocellulosic Biomass. *Waste and Biomass Valorization* **2021**, *12*, 2145–2169.

(11) Zhu, X.; Liu, Y.; Luo, G.; Qian, F.; Zhang, S.; Chen, J. Facile Fabrication of Magnetic Carbon Composites from Hydrochar via Simultaneous Activation and Magnetization for Triclosan Adsorption. *Environ. Sci. Technol.* **2014**, *48*, 5840–5848.

(12) Carpenter, A. W.; De Lannoy, C. F.; Wiesner, M. R. Cellulose Nanomaterials in Water Treatment Technologies. *Environ. Sci. Technol.* **2015**, *49*, 5277–5287.

(13) Varma, R. S. Biomass-Derived Renewable Carbonaceous Materials for Sustainable Chemical and Environmental Applications. *ACS Sustain. Chem. Eng.* **2019**, *7*, 6458–6470.

(14) Anirudhan, T. S.; Senan, P. Adsorption of Phosphate Ions from Water Using a Novel Cellulose-Based Adsorbent. *Chem. Ecol.* **2011**, *27*, 147–164.

(15) Hong, M.; Li, D.; Wang, B.; Zhang, J.; Peng, B.; Xu, X.; Wang, Y.; Bao, C.; Chen, J.; Zhang, Q. Cellulose-Derived Polyols as High-Capacity Adsorbents for Rapid Boron and Organic Pollutants Removal from Water. *J. Hazard. Mater.* **2021**, *419*, 126503.

(16) Ee, L. Y.; Chia, S. Y. R.; Xue, K.; Chin, S. Y.; Cho, C. A. H.; Tan, X. Y.; Li, S. F. Y. Hyperbranched Nanocellulose Enabling Rapid Boron Removal from Aqueous Environment. *Chem. Eng. J.* **2023**, *454*, 140218.

(17) Alongi, J.; Malucelli, G. Cotton Flame Retardancy: State of the Art and Future Perspectives. *RSC Adv.* **2015**, *5*, 24239–24263.

(18) Donmez Cavdar, A.; Mengeloɨlu, F.; Karakus, K. Effect of Boric Acid and Borax on Mechanical, Fire and Thermal Properties of Wood Flour Filled High Density Polyethylene Composites. *Meas. J. Int. Meas. Confed.* **2015**, *60*, 6–12.

(19) Yang, H.; Yu, B.; Xu, X.; Bourbigot, S.; Wang, H.; Song, P. Lignin-Derived Bio-Based Flame Retardants toward High-Performance Sustainable Polymeric Materials. *Green*

Chem. **2020**, *22*, 2129–2161.

(20) Uddin, K. M. A.; Ago, M.; Rojas, O. J. Hybrid Films of Chitosan, Cellulose Nanofibrils and Boric Acid: Flame Retardancy, Optical and Thermo-Mechanical Properties. *Carbohydr. Polym.* **2017**, *177*, 13–21.

(21) Mohamed, A. L.; Hassabo, A. G. Flame Retardants: Edition: 1. In *Flame Retardant of Cellulosic Materials and Their Composites*; 2015; pp 247–314.

(22) Yang, Z. W.; Liang, X. X.; Xu, X. Q.; Lei, C.; He, X. L.; Song, T.; Huo, W. Y.; Ma, H. C.; Lei, Z. Q. PGS@B-N: An Efficient Flame Retardant to Improve Simultaneously the Interfacial Interaction and the Flame Retardancy of EVA. *RSC Adv.* **2016**, *6*, 65921–65929.

(23) Zhang, J.; Koubaa, A.; Xing, D.; Liu, W.; Wang, Q.; Wang, X. M.; Wang, H. Improving Lignocellulose Thermal Stability by Chemical Modification with Boric Acid for Incorporating into Polyamide. *Mater. Des.* **2020**, *191*, 108589.

(24) Vicente Esquivel-Pena, Valentina Guccini, Sugam Kumar, G. S.-; Alvarez, Eduardo Rodr´ıguez de San Miguel, J. de G. Hybrids Based on Borate-Functionalized Cellulose Nanofibers and Noble-Metal Nanoparticles as Sustainable Catalysts for Environmental Applications. *RSC Adv.* **2020**, *10*, 12460–12468.

(25) Zhang, L.; Ding, Y.; Song, J. Crosslinked Carboxymethyl Cellulose-Sodium Borate Hybrid Binder for Advanced Silicon Anodes in Lithium-Ion Batteries. *Chinese Chem. Lett.* **2018**, *29*, 1773–1776.

(26) Lim, J. Y. C.; Goh, S. S.; Liow, S. S.; Xue, K.; Loh, X. J. Molecular Gel Sorbent Materials for Environmental Remediation and Wastewater Treatment. *J. Mater. Chem. A* **2019**, *7*, 18759–18791.

(27) Notley, S. M.; Chen, W.; Pelton, R. Extraordinary Adhesion of Phenylboronic Acid

Derivatives of Polyvinylamine to Wet Cellulose: A Colloidal Probe Microscopy Investigation. *Langmuir* **2009**, *25*, 6898–6904.

(28) Nawaz, H.; Zhang, J.; Tian, W.; Jin, K.; Jia, R.; Yang, T. Cellulose-Based Fluorescent Sensor for Visual and Versatile Detection of Amines and Anions. *J. Hazard. Mater.* **2020**, *387*, 121719.

(29) Kim, J.; Yun, S.; Mahadeva, S. K.; Yun, K.; Yang, S. Y.; Maniruzzaman, M. Paper Actuators Made with Cellulose and Hybrid Materials. *Sensors* **2010**, *10*, 1473–1485.

(30) Wang, B.; Guo, X.; Bai, P. Removal Technology of Boron Dissolved in Aqueous Solutions - A Review. *Colloids and Surfaces A: Physicochemical and Engineering Aspects*. Elsevier B.V. March 5, 2014, pp 338–344.

(31) Rodríguez Pastor, M.; Ferrándiz Ruiz, A.; Chillón, M. F.; Prats Rico, D. Influence of PH in the Elimination of Boron by Means of Reverse Osmosis. *Desalination* **2001**, *140*, 145–152.

(32) Bandura-Zalska, B.; Dydo, P.; Turek, M. Desalination of Boron-Containing Wastewater at No Boron Transport. *Desalination* **2009**, *241*, 133–137.

(33) Yilmaz, A. E.; Boncukcuoğlu, R.; Kocakerim, M. M.; Yilmaz, M. T.; Paluluoğlu, C. Boron Removal from Geothermal Waters by Electrocoagulation. *J. Hazard. Mater.* **2008**, *153*, 146–151.

(34) Liao, X.; Zhang, Q. Mesoporous Polymer Nanosponges Immobilized with Functional Polyols for Rapid Removal of Boric Acid and Organic Micropollutants. *ACS Appl. Polym. Mater.* **2019**, *1*, 2089–2098.

(35) Hilal, N.; Kim, G. J.; Somerfield, C. Boron Removal from Saline Water: A Comprehensive Review. *Desalination* **2011**, *273*, 23–35.

(36) Kluczka, J.; Pudło, W.; Krukiewicz, K. Boron Adsorption Removal by Commercial and

Modified Activated Carbons. *Chem. Eng. Res. Des.* **2019**, *147*, 30–42.

(37) Tang, Y. P.; Chung, T. S.; Weber, M.; Maletzko, C. Development of Novel Diol-Functionalized Silica Particles toward Fast and Efficient Boron Removal. *Ind. Eng. Chem. Res.* **2017**, *56*, 11618–11627.

(38) Ezechi, E. H.; Isa, M. H.; Mohamed Kutty, S. R. Bin. Boron in Produced Water: Challenges and Improvements: A Comprehensive Review. *J. Appl. Sci.* **2012**, *12*, 402–415.

(39) Nasef, M. M.; Nallappan, M.; Ujang, Z. Polymer-Based Chelating Adsorbents for the Selective Removal of Boron from Water and Wastewater: A Review. *React. Funct. Polym.* **2014**, *85*, 54–68.

(40) Peters, J. A. Interactions between Boric Acid Derivatives and Saccharides in Aqueous Media: Structures and Stabilities of Resulting Esters. *Coord. Chem. Rev.* **2014**, *268*, 1–22.

(41) Liao, X.; Wang, B.; Zhang, Q. Synthesis of Glycopolymer Nanosponges with Enhanced Adsorption Performances for Boron Removal and Water Treatment. *J. Mater. Chem. A* **2018**, *6*, 21193–21206.

(42) Miyazaki, Y.; Matsuoka, S.; Asada, K.; Kawasaki, Y.; Yoshimura, K. Interaction of Borate and Phenylboronate with the Cross-Linked Dextran Gel Matrix. *Polyhedron* **2018**, *151*, 233–242.

(43) Wei, Y. T.; Zheng, Y. M.; Chen, J. P. Functionalization of Regenerated Cellulose Membrane via Surface Initiated Atom Transfer Radical Polymerization for Boron Removal from Aqueous Solution. *Langmuir* **2011**, *27*, 6018–6025.

(44) Bursalı, E. A.; Seki, Y.; Seyhan, S.; Delener, M.; Yurdakoç, M. Synthesis of Chitosan Beads as Boron Sorbents. *J. Appl. Polym. Sci.* **2011**, *122*, 657–665.

(45) Sacco, P.; Furlani, F.; Cok, M.; Travan, A.; Borgogna, M.; Marsich, E.; Paoletti, S.;

Donati, I. Boric Acid Induced Transient Cross-Links in Lactose-Modified Chitosan (Chitlac). *Biomacromolecules* **2017**, *18*, 4206–4213.

(46) Li, D.; Chen, Y.; Liu, Z. Boronate Affinity Materials for Separation and Molecular Recognition: Structure, Properties and Applications. *Chem. Soc. Rev.* **2015**, *44*, 8097–8123.

(47) Tongye, S.; Langan, P.; French, A. D.; Johnson, G. P.; Gnanakaran, S. Conformational Flexibility of Soluble Cellulose Oligomers: Chain Length and Temperature Dependence. *J. Am. Chem. Soc.* **2009**, *131*, 14786–14794.

(48) Anggara, K.; Zhu, Y.; Fittolani, G.; Yu, Y.; Tyrikos-Ergas, T.; Delbianco, M.; Rauschenbach, S.; Abb, S.; Seeberger, P. H.; Kern, K. Identifying the Origin of Local Flexibility in a Carbohydrate Polymer. *Proc. Natl. Acad. Sci.* **2021**, *118*, e2102168118.

(49) Park, S.; Baker, J. O.; Himmel, M. E.; Parilla, P. A.; Johnson, D. K. Cellulose Crystallinity Index: Measurement Techniques and Their Impact on Interpreting Cellulase Performance. *Biotechnol. Biofuels* **2010**, *3*, 10.

(50) Schenzel, K.; Fischer, S.; Brendler, E. New Method for Determining the Degree of Cellulose I Crystallinity by Means of FT Raman Spectroscopy. *Cellulose* **2005**, *12*, 223–231.

(51) Earl, W. L.; VanderHart, D. L. High Resolution, Magic Angle Sample Spinning 13C NMR of Solid Cellulose I. *J. Am. Chem. Soc.* **1980**, *102* (9), 3251–3252.

(52) Kolodziejski, W.; Frye, J. S.; Maclel, G. E. Carbon-13 Nuclear Magnetic Resonance Spectrometry with Cross Polarization and Magic-Angle Spinning for Analysis of Lodgepole Pine Wood. *Anal. Chem.* **1982**, *54* (8), 1419–1424.

(53) Lesage, A.; Bardet, M.; Emsley, L. Through-Bond Carbon-Carbon Connectivities in Disordered Solids by NMR. *J. Am. Chem. Soc.* **1999**, *121* (47), 10987–10993.

(54) Bardet, M.; Gerbaud, G.; Giffard, M.; Doan, C.; Hediger, S.; Le Pape, L. 13C High-Resolution Solid-State NMR for Structural Elucidation of Archaeological Woods. *Prog. Nucl. Magn. Reson. Spectrosc.* **2009**, *55*, 199–214.

(55) Foston, M. Advances in Solid-State NMR of Cellulose. *Curr. Opin. Biotechnol.* **2014**, *27*, 176–184.

(56) Gutmann, T.; Kumari, B.; Zhao, L.; Breitzke, H.; Schöttner, S.; Rüttiger, C.; Gallei, M. Dynamic Nuclear Polarization Signal Amplification as a Sensitive Probe for Specific Functionalization of Complex Paper Substrates. *J. Phys. Chem. C* **2017**, *121* (7), 3896–3903.

(57) Terrett, O. M.; Lyczakowski, J. J.; Yu, L.; Iuga, D.; Franks, W. T.; Brown, S. P.; Dupree, R.; Dupree, P. Molecular Architecture of Softwood Revealed by Solid-State NMR. *Nat. Commun.* **2019**, *10*, 4978.

(58) Kumar, A.; Durand, H.; Zeno, E.; Balsollier, C.; Watbled, B.; Sillard, C.; Fort, S.; Baussanne, I.; Belgacem, N.; Lee, D.; Hediger, S.; Demeunynck, M.; Bras, J.; De Paëpe, G. The Surface Chemistry of a Nanocellulose Drug Carrier Unravelled by MAS-DNP. *Chem. Sci.* **2020**, *11* (15), 3868–3877.

(59) Cresswell, R.; Dupree, R.; Brown, S. P.; Pereira, C. S.; Skaf, M. S.; Sorieul, M.; Dupree, P.; Hill, S. Importance of Water in Maintaining Softwood Secondary Cell Wall Nanostructure. *Biomacromolecules* **2021**, *22*, 4669–4680.

(60) Berruyer, P.; Moutzouri, P.; Gericke, M.; Jakobi, D.; Bardet, M.; Heinze, T.; Karlson, L.; Schantz, S.; Emsley, L. Spatial Distribution of Functional Groups in Cellulose Ethers by DNP-Enhanced Solid-State NMR Spectroscopy. *Macromolecules* **2022**, *55* (7), 2952–2958.

(61) Sanfeliu, C.; Martínez-Máñez, R.; Sancenón, F.; Soto, J.; Amorós, P.; Azaïs, T.; Marcos,

M. D. ^{11}B-MAS NMR Approach to the Boron Adsorption Mechanism on a Glucose-Functionalised Mesoporous Silica Matrix. *Microporous Mesoporous Mater.* **2018**, *266*, 232–241.

(62) Fung, B. M.; Khitrin, A. K.; Ermolaev, K. An Improved Broadband Decoupling Sequence for Liquid Crystals and Solids. *J. Magn. Reson.* **2000**, *142*, 97–101.

(63) Łdziana, Z.; Błoński, P.; Yan, Y.; Rentsch, D.; Remhof, A. NMR Chemical Shifts of 11B in Metal Borohydrides from First-Principle Calculations. *J. Phys. Chem. C* **2014**, *118*, 6594–6603.

(64) Lesage, A.; Sakellariou, D.; Hediger, S.; Eléna, B.; Charmont, P.; Steuernagel, S.; Emsley, L. Experimental Aspects of Proton NMR Spectroscopy in Solids Using Phase-Modulated Homonuclear Dipolar Decoupling. *J. Magn. Reson.* **2003**, *163* (1), 105–113.

(65) Wiench, J. W.; Bronnimann, C. E.; S-Y Lin, V.; Pruski, M. Chemical Shift Correlation NMR Spectroscopy with Indirect Detection in Fast Rotating Solids: Studies of Organically Functionalized Mesoporous Silicas. **2007**. https://doi.org/10.1021/ja074746.

(66) Manjunatha Reddy, G. N.; Gerbec, J. A.; Shimizu, F.; Chmelka, B. F. Nanoscale Surface Compositions and Structures Influence Boron Adsorption Properties of Anion Exchange Resins. *Langmuir* **2019**, *35* (48), 15661–15673.

(67) Yoshimura, K.; Miyazaki, Y.; Ota, F.; Matsuoka, S.; Sakashita, H. Complexation of Boric Acid with the N-Methyl-D-Glucamine Group in Solution and in Crosslinked Polymer. *J. Chem. Soc. - Faraday Trans.* **1998**, *94*, 683–689.

(68) Miyazaki, Y.; Yoshimura, K.; Miura, Y.; Sakashita, H.; Ishimaru, K. ^{11}B NMR Investigation of the Complexation Behavior of Borate with Polysaccharides in Aqueous Solution. *Polyhedron* **2003**, *22* (6), 909–916.

(69) Peters, G. M.; Skala, L. P.; Plank, T. N.; Oh, H.; Reddy, G. N. M.; Marsh, A.; Brown, S.

P.; Raghavan, S. R.; Davis, J. T. G4-Quartet·M+ Borate Hydrogels. *J. Am. Chem. Soc.* **2015**, *137*, 5819–5827.

(70) Peters, G. M.; Skala, L. P.; Plank, T. N.; Hyman, B. J.; Reddy, G. N. M.; Marsh, A.; Brown, S. P.; Davis, J. T. A G4·K+ Hydrogel Stabilized by an Anion. *J. Am. Chem. Soc.* **2014**, *136*, 12596–12599.

(71) Wicklein, B.; Kocjan, D.; Carosio, F.; Camino, G.; Bergström, L. Tuning the Nanocellulose-Borate Interaction to Achieve Highly Flame Retardant Hybrid Materials. *Chem. Mater.* **2016**, *28* (7), 1985–1989.

(72) Hušák, M.; Jegorov, A.; Rohlíček, J.; Fitch, A.; Czernek, J.; Kobera, L.; Brus, J. Determining the Crystal Structures of Peptide Analogs of Boronic Acid in the Absence of Single Crystals: Intricate Motifs of Ixazomib Citrate Revealed by XRPD Guided by Ss-NMR. *Cryst. Growth Des.* **2018**, *18*, 3616–3625.

(73) Kobera, L.; Czernek, J.; Strečková, M.; Urbanova, M.; Abbrent, S.; Brus, J. Structure and Distribution of Cross-Links in Boron-Modified Phenol-Formaldehyde Resins Designed for Soft Magnetic Composites: A Multiple-Quantum ^{11}B-^{11}B MAS NMR Correlation Spectroscopy Study. *Macromolecules* **2015**, *48*, 4874–4881.

(74) Bishop, M.; Shahid, N.; Yang, J.; Barron, A. R. Determination of the Mode and Efficacy of the Cross-Linking of Guar by Borate Using MAS ^{11}B NMR of Borate Cross-Linked Guar in Combination with Solution ^{11}B NMR of Model Systems. *Dalt. Trans.* **2004**, 2621–2634.

(75) Reddy, G. N. M.; Peters, G. M.; Tatman, B. P.; Rajan, T. S.; Kock, S. M.; Zhang, J.; Frenguelli, B. G.; Davis, J. T.; Marsh, A.; Brown, S. P. Magic-Angle Spinning NMR Spectroscopy Provides Insight into the Impact of Small Molecule Uptake by G-Quartet Hydrogels. *Mater. Adv.* **2020**, *1*, 2236–2247.

(76) Bialik, E.; Stenqvist, B.; Fang, Y.; Östlund, Å.; Furó, I.; Lindman, B.; Lund, M.; Bernin, D. Ionization of Cellobiose in Aqueous Alkali and the Mechanism of Cellulose Dissolution. *J. Phys. Chem. Lett.* **2016**, *7* (24), 5044–5048.

(77) Zhao, G.; Wang, F.; Lang, X.; He, B.; Li, J.; Li, X. Facile One-Pot Fabrication of Cellulose Nanocrystals and Enzymatic Synthesis of Its Esterified Derivative in Mixed Ionic Liquids. *RSC Adv.* **2017**, *7*, 27017–27023.

(78) Gast, J. C.; Atalla, R. H.; McKelvey, R. D. The ^{13}C-N.M.R. Spectra of the Xylo- and Cello-Oligosaccharides. *Carbohydr. Res.* **1980**, *84*, 137–146.

(79) Katahira, R.; Elder, T. J.; Beckham, G. T. A Brief Introduction to Lignin Structure. In *Lignin Valorization: Emerging Approaches*; The Royal Society of Chemistry, 2018; pp 1–20.

(80) Sasaki, K.; Qiu, X.; Miyawaki, J.; Ideta, K.; Takamori, H.; Moriyama, S.; Hirajima, T. Contribution of Boron-Specific Resins Containing N-Methylglucamine Groups to Immobilization of Borate/Boric Acid in a Permeable Reactive Barrier Comprising Agglomerated MgO. *Desalination* **2014**, *337*, 109–116.

Electronic Supplementary Information for:

Boron adsorption kinetics of microcrystalline cellulose and polymer resin

Parth Raval, Neethu Thomas, Lama Hamdouna, Laurent Delevoye, Olivier Lafon, and G. N. Manjunatha Reddy*

University of Lille, CNRS, Centrale Lille Institut, Univ. Artois, UMR 8181−UCCS− Unité de Catalyse et Chimie du Solide, F-59000, Lille, France

*corresponding author: gnm.reddy@univ-lille.fr

Table of Contents

1. Structures of polystyrene divinylbenzene based resins

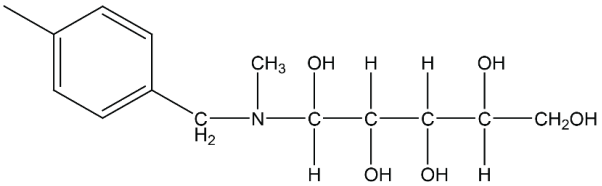

DOWEX XUS-43594.00

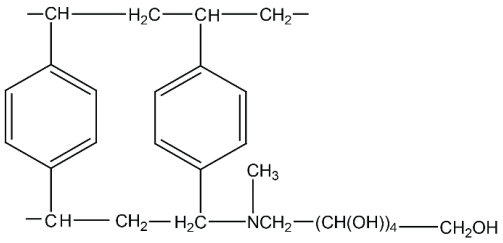

Diaion CRB 02

Figure S1. Chemical structures of Dowex and Diaion CRB-02 resins.

2. Liquid state ^{11}B NMR spectra of boron-treated lignin

Figure S2 shows the liquid state ^{11}B NMR spectra of lignin treated with boric-acid solution (33.2 g/L) displayed on top and the pristine boric acid solution (33.2 g/L) shown at the bottom. For both solutions, the pH was maintained at 11 by the addition of stoichiometric concentration of NaOH solution to the boric acid solution. Both samples exhibit identical ^{11}B shifts at 1-2.5 ppm, which could be attributed to the formation of metal-borate agglomerates in solution.

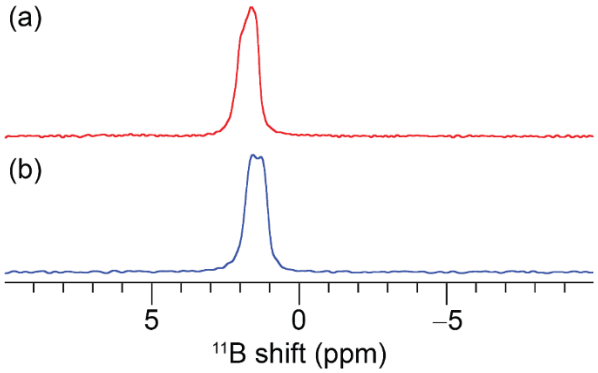

Figure S2. Liquid-state ^{11}B NMR spectra of pH-controlled (a) boric acid treated lignin and (b) boric acid solution. All spectra were acquired at 9.4 T (^{1}H = 400 MHz and ^{11}B = 128.4 MHz) under a static condition.

3. FT-IR spectra of neat cellulose and boron-treated cellulose

Figure S2 presents the FT-IR spectra of untreated and boric acid-treated cellulose. The vibrational band at (1) ~3300 cm^{-1} is attributed to the free O-H stretching frequency of hydroxyl groups, and those at (2) 2920 cm^{-1} and (4) 1420 cm^{-1} correspond to C-H bending and stretching frequencies in cellulose, respectively.[1] Trigonal BO and tetragonal BO are known to have bending frequencies at approximately 1470 cm^{-1} (3) and 970 cm^{-1} (6), respectively.[2] The peaks around 1040 cm^{-1} (5) and 870 cm^{-1} (7) corresponded to the C-O-C stretching vibration of the pyranose ring.[3,4]

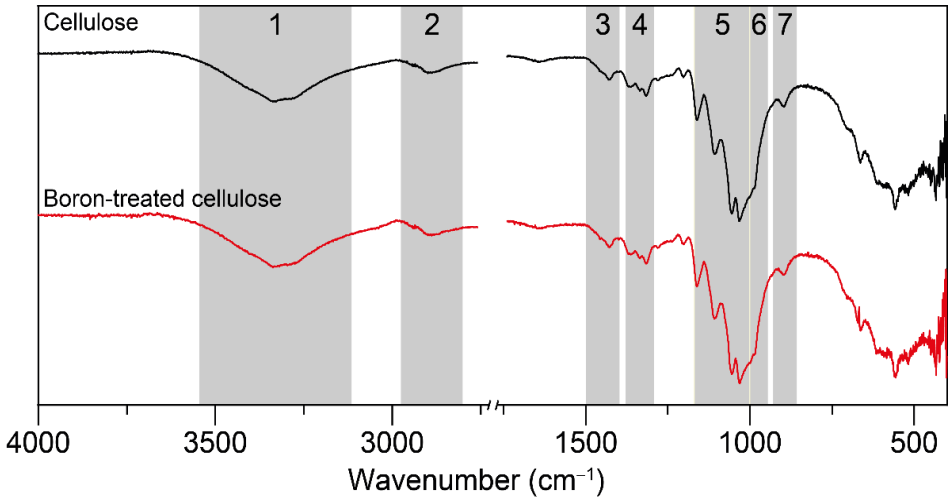

Figure S3. Solid-state ATR FT-IR transmittance plots of pristine cellulose and boric acid-treated cellulose acquired at room temperature.

4. 1D ^{11}B NMR spectra of boron adsorbed cellulose acquired at variable MAS frequency

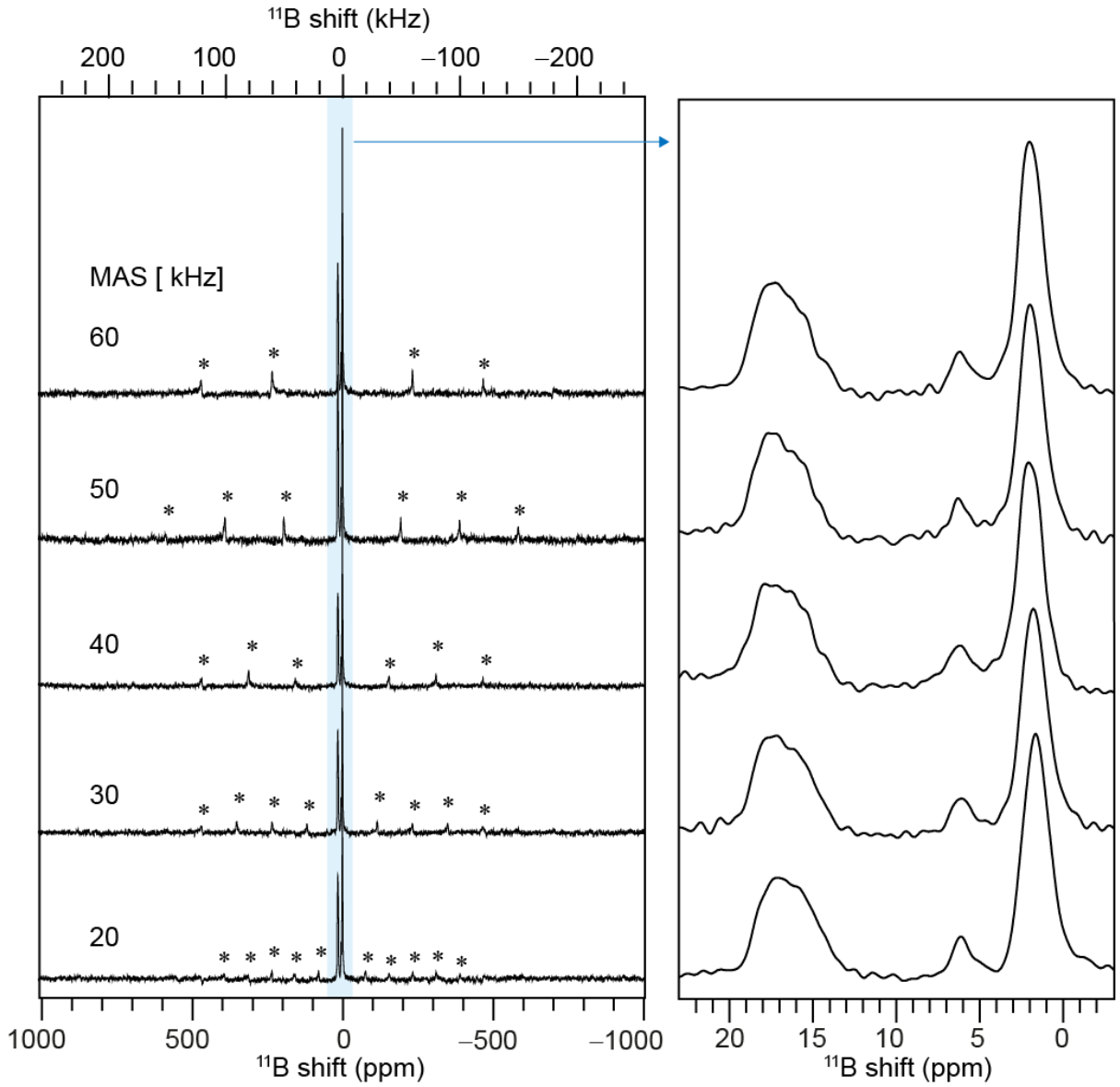

Figure S4. Solid-state 1D ^{11}B MAS NMR spectra of boron adsorbed cellulose (left) acquired at 18.8 T (Larmor frequency of ^{11}B = 256.7 MHz) using a Hahn echo sequence at variable MAS frequencies as indicated alongside the spectrum. Spinning sidebands are denoted by asterisks. The expanded region of the same ^{11}B MAS spectra are shown in the right-hand-side panel, whereby no further line narrowing is observed with increasing MAS, suggesting that the obtained line narrowing at 18.8 T compared to 9.4 T is primarily due to the reduced second order quadrupolar interactions that are inversely proportional to the magnetic field strength.

5. Solid-state 1D ^{23}Na NMR spectrum of boron-treated cellulose

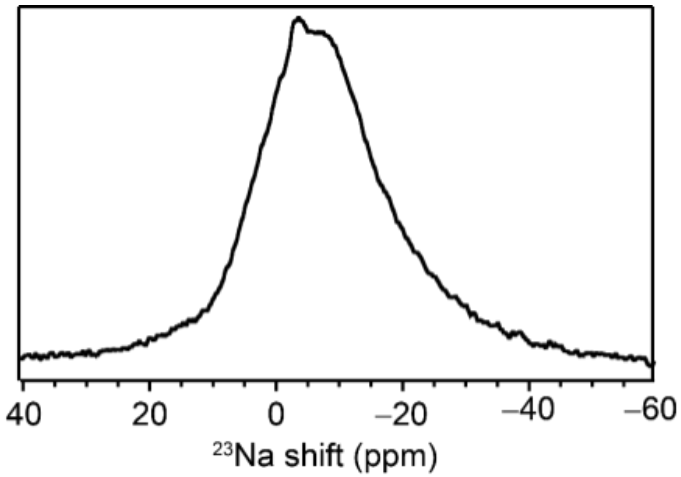

Figure S5. Solid-state 1D ^{23}Na MAS NMR spectrum of boric acid-treated cellulose acquired at 9.4 T, and 8 kHz MAS.

6. 1D $^{11}B\{^{1}H\}$ CP-MAS spectra of boron adsorbed cellulose and CP buildup curves

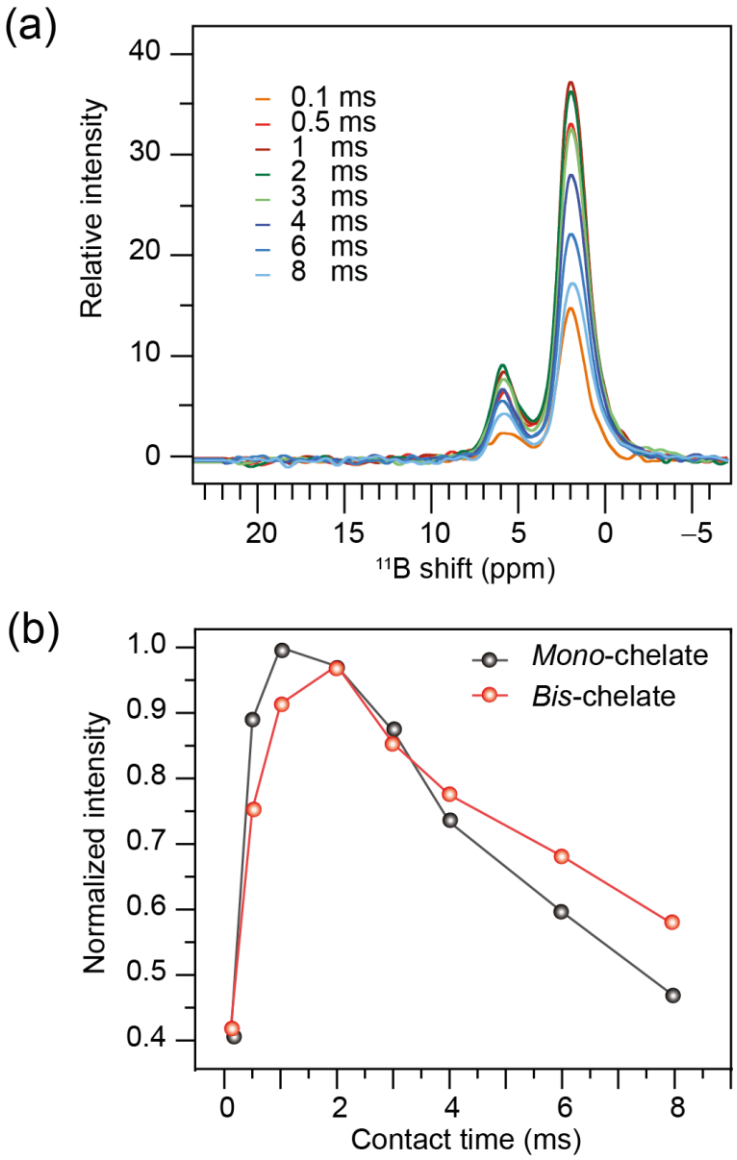

Figure S6. (a) The $^{11}B\{^{1}H\}$ CPMAS NMR spectra of boron-treated cellulose acquired at 9.4 T and 8 kHz MAS frequency using a dedicated 4 mm HX probe to eliminate the ^{11}B background signal**.** The boric acid concentration was 33.8 g/L. (b) A plot of normalized ^{11}B intensity of *mono*-chelate complexes (black dots) and *bis*-chelate complexes (red dots) as a function of CP contact time (from 0.1 ms to 8 ms) for boron-treated cellulose obtained from $^{11}B\{^{1}H\}$ CP-MAS NMR spectra. Although *mono*-chelate complexes show a faster CP build up owing to stronger dipolar couplings due to its proximity to hydroxyl protons, it can be seen that the optimal contact time for *mono*-chelate signal is 1 ms due to the presence of labile -OH groups, but 2 ms for *bis*-chelate peaks.

7. 1D ^{11}B NMR spectra of boron adsorbed cellulose before and after washing with water

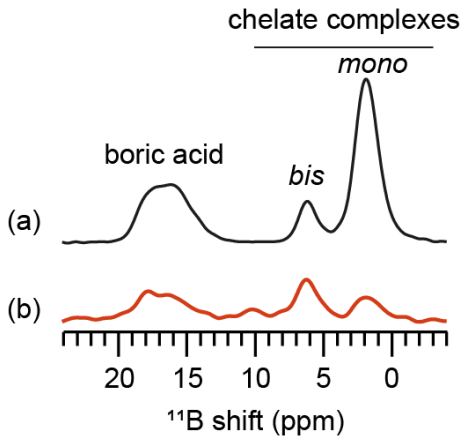

Figure S7. Solid-state 1D ^{11}B MAS NMR spectra of boron-treated cellulose acquired (a) before and (b) after washing with Millipore water. All spectra were acquired at 18.8 T and 50 kHz MAS frequency**.** The cellulose powder was treated with aqueous solution of boric acid (33.8 g/L), centrifuged and dried prior to the acquisition of ^{11}B MAS NMR spectrum shown in (a), and the same material is washed subsequently with water for three times, dried and ^{11}B MAS NMR spectrum was acquired as shown in (b).

8. Lineshape analysis of ^{11}B NMR spectrum of boron-treated cellulose

Table S1. Best-fit ^{11}B MAS NMR parameters, δ_{iso}, C_Q, and η_Q[a], for distinct boron sites in boric acid-treated cellulose as a function of boric acid concentration at pH = 11.

Conc. of boric acid (g/L)	*Mono*-chelate complex			*Bis*-chelate complex			Unreacted boric acid		
	δ_{iso} (ppm)	C_Q (MHz)	η_Q	δ_{iso} (ppm)	C_Q (MHz)	η_Q	δ_{iso} (ppm)	C_Q (MHz)	η_Q
5.8	1.9	0.2	0.01	5.9	0.2	0.01	18.6	2.2	0.34
11.6	1.9	0.3	0.01	5.9	0.3	0.02	18.6	2.3	0.18
22.7	1.9	0.4	0.01	5.9	0.4	0.02	18.6	2.4	0.11
33.8	1.9	0.4	0.01	5.9	0.4	0.02	18.6	2.4	0.14
67.2	1.9	0.4	0.01	5.9	0.4	0.02	18.6	2.4	0.18
134.2	1.9	0.5	0.02	5.9	0.4	0.02	18.6	2.4	0.19

[a] Errors on the δ_{iso}, C_Q, and η_Q are estimated as ±0.1 ppm, 0.1 MHz, and 0.01, respectively.

Table S2. Best-fit ^{11}B MAS NMR parameters, δ_{iso}, C_Q, and η_Q[a], of distinct boron sites in boric acid, treated cellulose as a function of pH at a boric acid concentration of 33.5 g.L^{-1}.

pH	*Mono*-chelate complex			*Bis*-chelate complex			Unreacted boric acid		
	δ_{iso} (ppm)	C_Q (MHz)	η_Q	δ_{iso} (ppm)	C_Q (MHz)	η_Q	δ_{iso} (ppm)	C_Q (MHz)	η_Q
13	1.9	0.3	0.01	5.9	0.3	0.02	18.2	2.4	0.15
11	1.9	0.4	0.02	5.9	0.4	0.02	18.6	2.4	0.14
9	1.9	0.4	0.02	5.9	0.7	0.02	18.6	2.4	0.01
7	1.9	0.9	0.02	5.9	0.5	0.02	18.6	2.5	0.25
5	1.9	0.8	0.02	5.9	0.8	0.02	18.6	2.3	0.15

[a] Errors on the δ_{iso}, C_Q, and η_Q are estimated as ±0.1 ppm, 0.1 MHz, and 0.01, respectively.

9. Estimation of boron present in the supernatant solution of cellulose

Concentration of boron species that are not adsorbed on the cellulose was estimated by analyzing the supernatant of boron treated cellulose powder using solution state ^{11}B NMR spectroscopy. The supernatant obtained by treating 80 mg cellulose with 1 mL of boric acid solution, each containing different concentration of boric acid 5.8, 33.8 and 134.2 g/L. After centrifugation (3 times), in each case 80 µL of supernatant was taken into the rotor. An aqueous solution of 0.5 M H_3BO_3 (pH 11) was used as an external standard which corresponds to 30.9 mg of boron per mL. The total area in the ^{11}B MAS spectrum of the 80 µL of boric acid solution was used as a calibration method, and the integrals corresponding to the boron peaks of 80 µL of the supernatants (i.e., excess of boron unreacted with cellulose and leached into the solution) were compared in order to estimate the mass of boron present in the supernatant solutions. Based on this analysis, 80 mg of cellulose treated with 5.8 mg boric acid (in 1 mL) yield to ~0.11 mg of boron adsorbed on the sorbent and ~5.69 mg of boron was leached into the supernatant (1 mL), which indicates that ~1.3 mg of boron captured by a gram of cellulose. For 80 mg of cellulose powder treated with 33.8 mg/mL boric acid solution, the mass of boron leached in to the solution is presented in **Table S3**, however, it excludes the unreacted boric acid precipitated in the cellulose sorbate. When boric acid solution greater than 33.8 mg/mL, unreacted boron acid precipitates in the network of cellulose (**Figure 2**, main manuscript).

Table S3. Mass of boron leached into the solution during the centrifugation process.

Mass of boric acid used (/mL) with 80 mg of cellulose	Volume of supernatant (µL)	Peak Integral (a.u.)	Mass of boron in 80 µL of solution (mg)	Mass of boron (mg/mL)
30.9 (neat boric acid)	80	1	2.47	30.91
5.8	80	0.1841	0.455	5.69
33.8	80	1.0028	2.48	31.00

10. Solid-state 1D ^{1}H, ^{13}C{^{1}H} and 2D ^{1}H-^{13}C HETCOR NMR spectra of neat cellulose

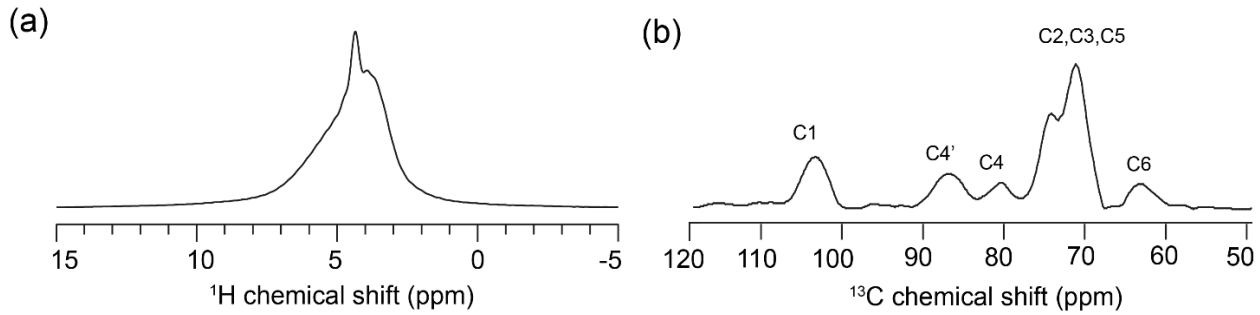

Figure S8. Solid-state (a) 1D ^{1}H MAS and (b) 1D ^{13}C{^{1}H} CP-MAS NMR spectra of pure cellulose acquired at 18.8 T with 50 kHz MAS using a CP contact time of 2 ms.

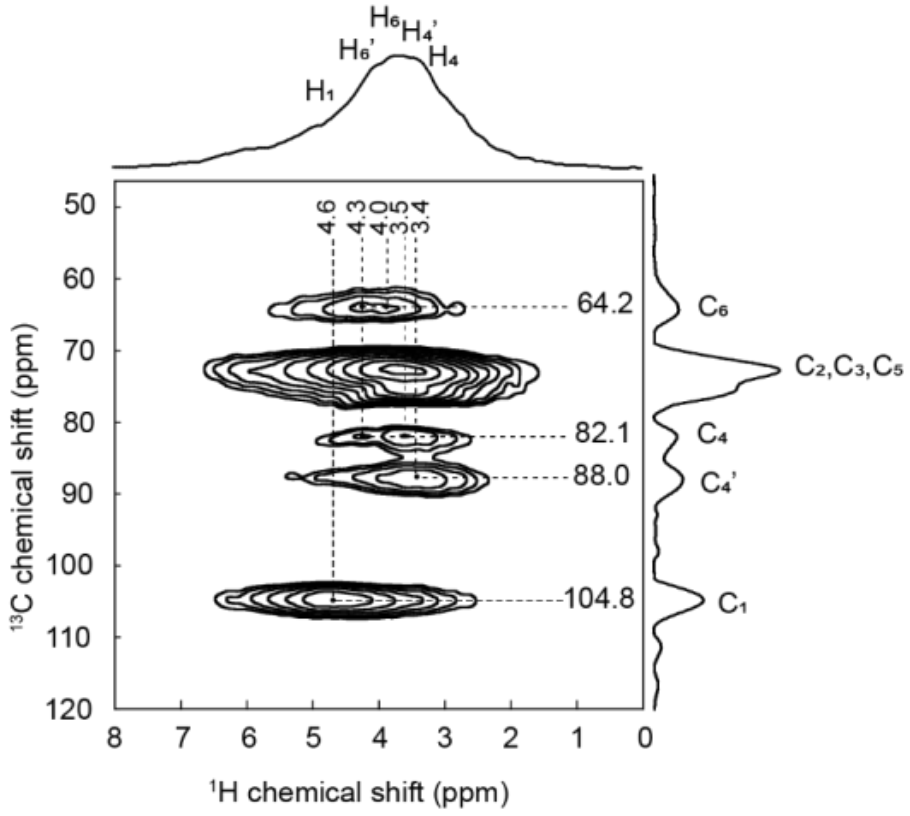

Figure S9. Solid-state 2D ^{13}C-^{1}H heteronuclear correlation NMR spectrum of pure cellulose acquired at 18.8 T with 50 kHz MAS using a CP contact time of 2 ms. Dashed lines depict the assignments of 2D ^{1}H-^{13}C correlation intensities.

11. Projections of 2D ^{13}C-^{1}H and ^{11}B-^{1}H HETCOR spectra of boron adsorbed cellulose

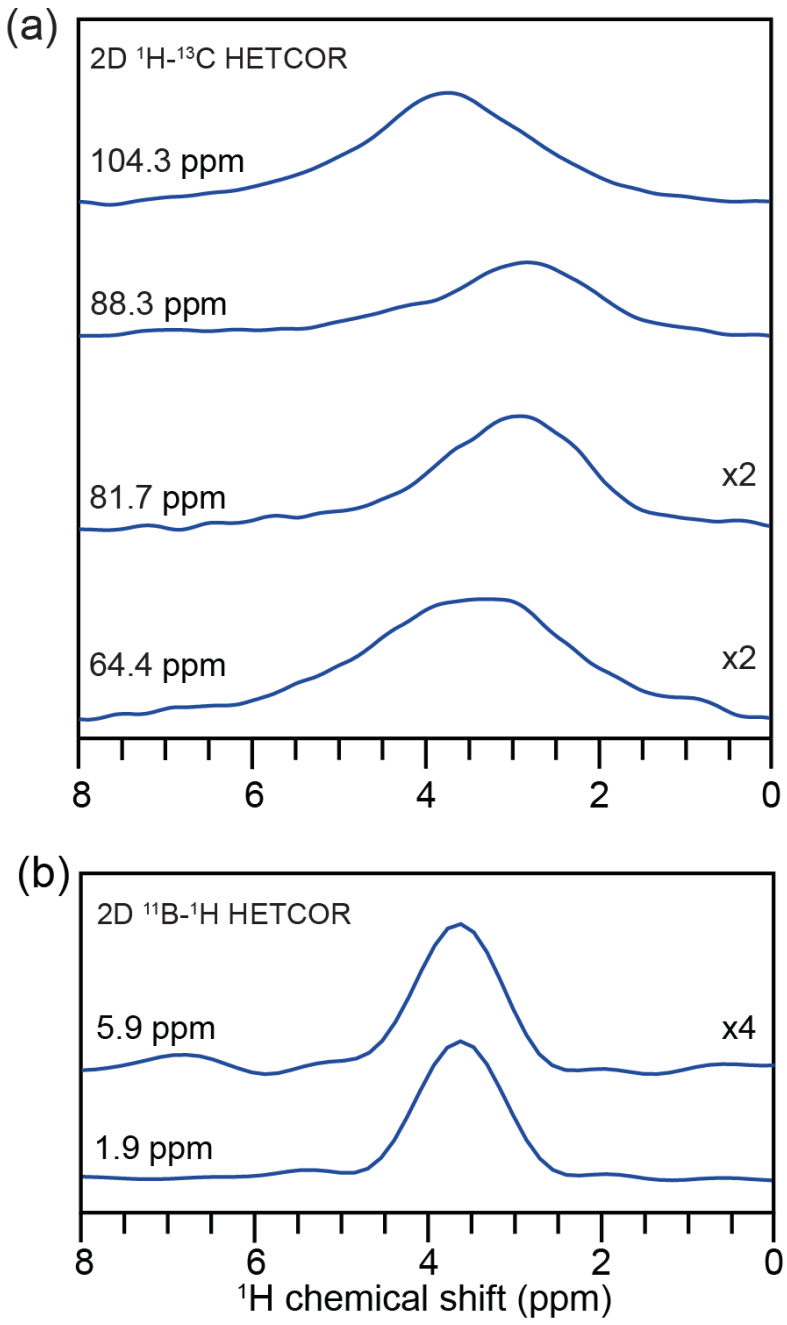

Figure S10. (a) Line-cut row spectra of ^{1}H chemical shifts extracted from a 2D ^{1}H-^{13}C heteronuclear correlation spectrum of cellulose at special ^{13}C signals as indicated in the inset and (b) column ^{1}H spectra obtained from 2D ^{11}B-^{1}H heteronuclear correlation NMR spectra for the ^{11}B signals associated with *mono*- and *bis*-chelate complexes.

12. Line shape analysis of ^{11}B NMR spectrum of boron-treated Amberlite IRA743

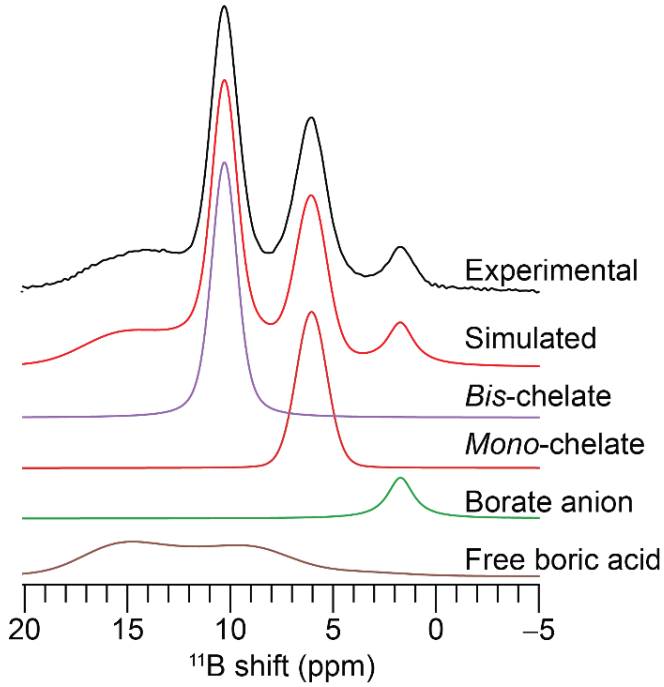

Figure S11. Solid-state 1D ^{11}B MAS NMR spectrum (top) of boric acid treated Amberlite IRA743 acquired with ^{1}H-decoupling at 9.4 T, room temperature and 8 kHz MAS. Deconvoluted signal intensities correspond to *mono*- and *bis*-chelate complexes, borate anion, and free boric acid.

Table S4. ^{11}B best-fit NMR parameters, δ_{iso}, C_Q, and η_Q of distinct boron sites in Amberlite IRA743 treated with 33.8 gL^{-1} boric acid at pH = 11.

Boron species	δ_{iso} (ppm)	C_Q (MHz)	η_Q
Borate anion	1.6	0.15	0.03
Mono-chelate	6.0	0.19	0.20
Bis-chelate	10.2	0.20	0.03
Free boric acid	18.8	2.13	0.17

Errors on the δ_{iso}, C_Q, and η_Q are estimated as ±0.1 ppm, ±0.1 MHz, and ±0.01, respectively.

13. Boron adsorption kinetics of Amberlite IRA743

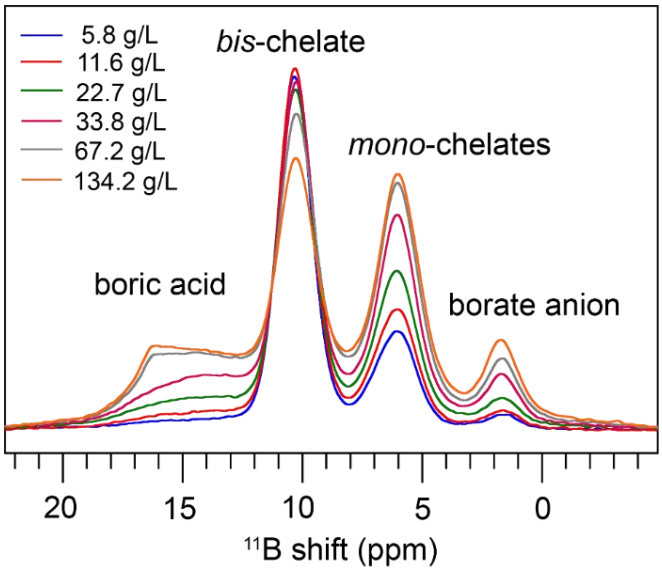

Figure S12. Comparison of 1D $^{11}B\{^{1}H\}$ MAS NMR spectra of Amberlite IRA743 resin treated with different concentrations of boric acid. All spectra were acquired at 9.4 T with 8 kHz MAS frequency at room temperature.

14. Comparison of boron adsorption kinetics of Amberlite IRA743 and cellulose

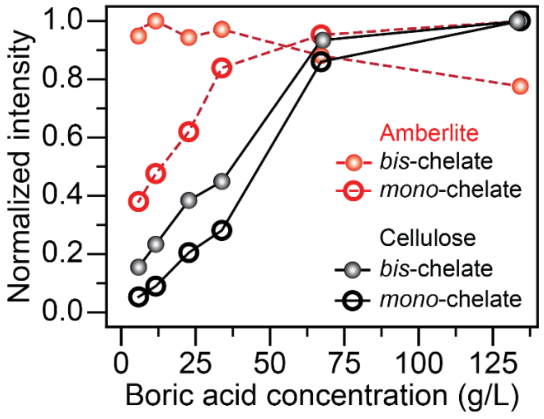

Figure S13. Normalized integrated intensities of the signal corresponding to the *mono*-chelate (marked as rings) and *bis*-chelate (marked as spheres) obtained from ^{11}B MAS NMR spectrum of boric acid treated cellulose and Amberlite IRA743 with respect to different boric acid concentrations acquired at 9.4 T and 8 kHz MAS.

15. Estimation of boron adsorption capacities of lignin, cellulose, and IRA743

Boron adsorption capacities of lignin, cellulose, and Amberlite were estimated by analyzing the ^{11}B NMR spectra of these materials acquired under similar conditions. For the ssNMR analysis, 100 mg of samples treated with 5.8 g/L of boric acid were used. This corresponds to ~1.0 mg of boron atoms estimated based on the atomic wt.% for 5.8 g/L concentration of boric acid in 1 mL of solution. For lignin, peaks corresponding to chelate complexes were not detected in the solution NMR spectra. For Amberlite and cellulose, 40 mg of the sample was weighed and packed in the rotors. Amberlite IRA743, the total area under the peaks at 1.5, 6.0 and 10.2 ppm in the ^{11}B MAS spectrum was calibrated to unity, which corresponds to ~0.4 mg boron (i.e., for 40 mg of the boric acid treated sorbent in the rotor), assuming that all the boron atoms were adsorbed. For 40 mg of boron adsorbed cellulose taken in a rotor, the peak integrals corresponding to *mono*- and *bis*-chelate boron sites in a ^{11}B MAS NMR spectrum (acquired at identical conditions) were measured and compared with Amberlite. Based on this analysis, the boron adsorption capacity of cellulose is estimated to be ~15% of that of Amberlite.

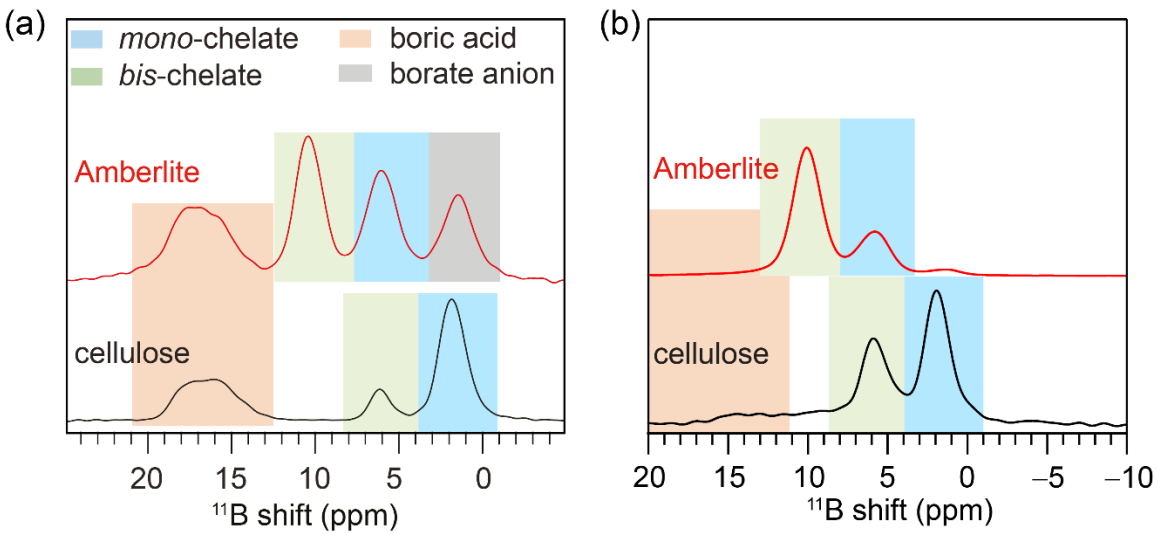

Figure S14. (a) 1D ^{11}B MAS NMR spectra of cellulose and Amberlite IRA743 treated with 5.8 mg boric acid, acquired at 18.8 T with 50 kHz MAS and (b) 1D ^{11}B{^{1}H} MAS NMR spectra of the same materials treated with 5.8 mg boric acid at 9.4 T and 8 kHz MAS. The blue and green-shaded boxes corresponding to *mono*-chelate and *bis*-chelate signals, respectively, as corroborated by the analysis of 2D ^{1}H-^{13}C and ^{11}B-^{1}H correlation NMR spectra.

As an alternative method using powdered $NaBH_4$ (wt.% of boron is 28.54%) as an external standard, the boron adsorption capacities of cellulose, and Amberlite were further estimated by acquiring and comparing the single-pulse ^{11}B NMR spectra of known concentration of $NaBH_4$ and boron adsorbed cellulose and Amberlite IRA743 materials obtained under identical acquisition conditions. Dried powders of boron adsorbed cellulose and Amberlite IRA743 materials were used to acquire the ^{11}B MAS NMR spectra at 18.8 T and 50 kHz MAS. The ^{11}B peak integral of $NaBH_4$ was calibrated to unity (2.9 mg of $NaBH_4$) and the integral corresponding to chelate boron sites in the spectra of both cellulose and Amberlite shown in **Figure S14** are compared with respect to this standard in order to estimate the boron adsorbed by cellulose and polymeric resin at the same concertation of boric acid used (33.8 mg/mL) for the reaction.

Table S5. The boron adsorption capacity of Amberlite IRA 743 and cellulose treated with 33.8 gL^{-1} boric acid at pH = 11.

Material	Mass of boron used to treat 80 mg sorbate in 1 mL (mg)	Sample mass in rotor taken for analysis (mg)	^{11}B peak integral[#]	Mass of boron in the rotor (mg)	Boron adsorbed (mg) / gram of sorbent
$NaBH_4$	---	2.9	1	0.83	---
Amberlite IRA743	33.8	2.6	0.06	0.11	17.2
4C cellulose	33.8	2.9	0.01	0.008	3.0

[#] Integrals of ^{11}B peaks associated with *mono*- and *bis*-chelate complexes are considered as boron adsorption sites. Contribution form the background signal for the ^{11}B MAS NMR spectra of sorbents acquired at 18.8 T with 1.3 mm HX probe is suppressed by subtracting the ^{11}B background signal acquired by an empty rotor under identical experimental condition.

16. Solid-state 1D ^{1}H and $^{13}C\{^{1}H\}$ NMR spectra of boron adsorbed resin

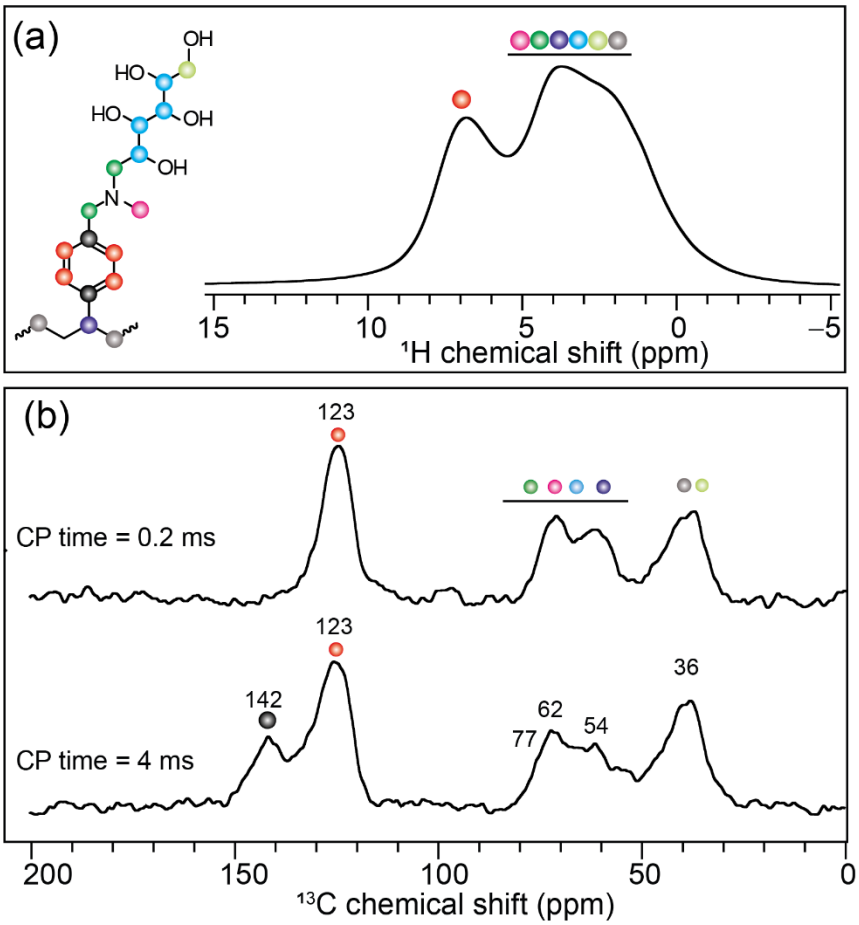

Figure S15. Solid-state 1D (a) ^{1}H MAS and (b) $^{13}C\{^{1}H\}$ CP-MAS NMR spectra of boric acid treated Amberlite IRA743 acquired at 18.8 T and 50 kHz MAS frequency. Spectral analysis is indicated by the color dots in the structure of polymeric resin Amberlite IRA743 (inset in the top).

Figure S15a displays a ^{1}H MAS spectrum of boron adsorbed resin with the color dots representing proton sites as depicted in the schematic structure. In the 1D $^{13}C\{^{1}H\}$ CP-MAS NMR spectrum of the same materials acquired with a short CP contact time of 0.2 ms (**Figure S15b**), signals at 30-50 ppm are due to methylene carbon sites in the polymer backbone and methylene groups bonded to amine group of NMDG moieties, and the broad distribution of peaks in the 55-80 ppm range are due to -NCH_2 and alkyl groups of NMDG sidechain. The ^{13}C signals in the 124-135 ppm range are due to aryl carbons in polymer backbone of resin. Additionally, the quaternary carbon sites (135-150 ppm) are observed in a $^{13}C\{^{1}H\}$ CP MAS spectrum acquired with 4 ms of contact time.

17. 2D ^{1}H-^{1}H DQ-SQ correlation NMR spectrum of boron adsorbed polymer resin

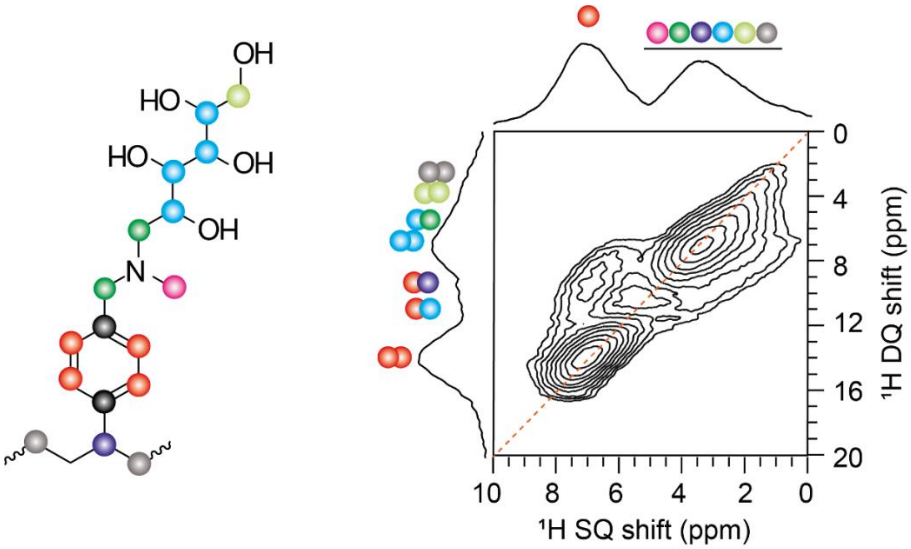

Figure S16. Solid-state 2D ^{1}H–^{1}H DQ-SQ correlation NMR spectra of boric acid treated Amberlite IRA743. Spectral analysis is indicated by the color dots as indicated in the structures shown in (a).

Figure S16 presents the ^{1}H DQ-SQ correlation spectrum of the boron adsorbed polymeric resin (Amberlite IRA743), together with the analysis of 1D ^{1}H MAS NMR spectrum with peaks corresponding to the aromatic protons and the different. DQ-SQ spectrum was acquired with Back-to-Back (BaBa) sequence with a DQ excitation time corresponding to 1 rotor period (τ_r = 20 μs). In the 2D ^{1}H–^{1}H DQ-SQ correlation NMR spectrum of boron-adsorbed resin, autocorrelation (i.e., on-diagonal) peaks are observed for -CH moieties of methylene groups in polymer backbone at ^{1}H(DQ) = (1.2 + 1.2) = 2.4 ppm, at ^{1}H(DQ) = (3.6 + 3.6) = 7.2 ppm for the -CH/CH_2/NCH_2/NHC_3 moieties of surface functionalized NMDG sidechains, and at ^{1}H(DQ) = 13.4 ppm, corresponding to the aromatic protons of the styrene backbone. The phenyl protons of polystyrene exhibits cross peaks with -NCH_3, -NCH_2 groups of NMDG side chain which indicate spatial proximity of these species. Relatively low intensity off-diagonal peaks between aromatic protons and NMDG moieties/CH_2 sites polystyrene chains are also detected.

18. 2D ^{11}B-^{1}H heteronuclear correlation spectra of boron adsorbed polymer resin

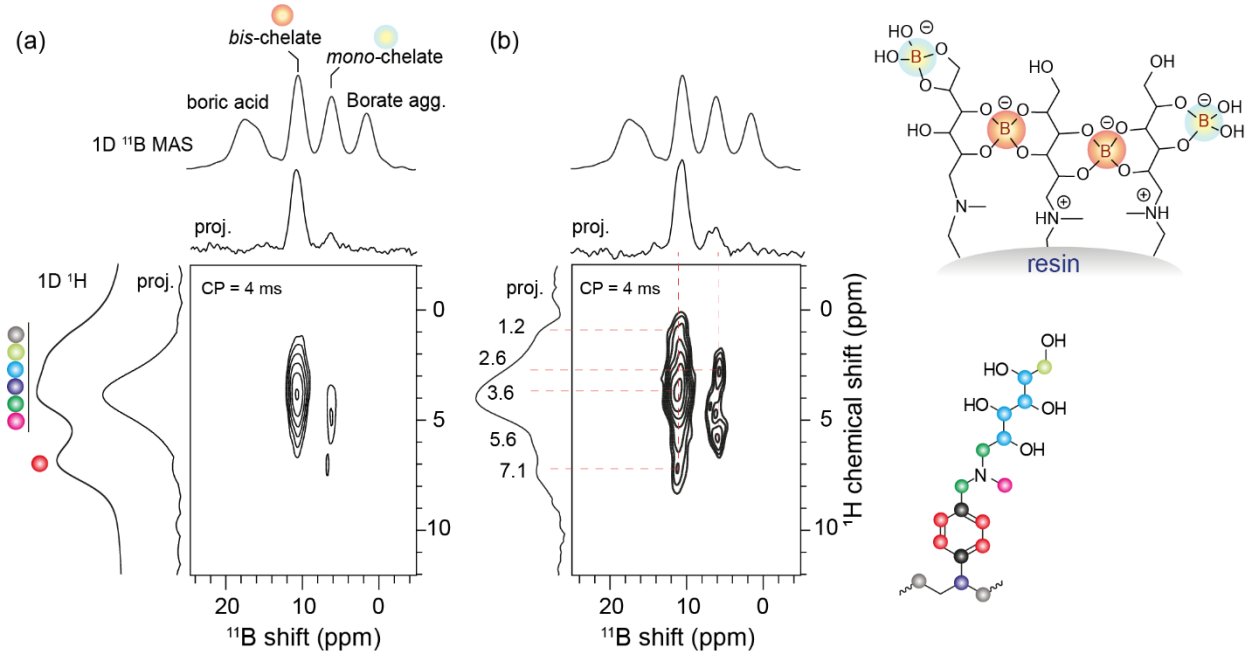

Figure S17. Solid-state 2D ^{11}B{^{1}H} HETCOR spectrum of boric acid treated Amberlite IRA743 acquired at 18.8 T and 50 kHz MAS frequency using a CP contact time of (a) 1 ms and (b) 4 ms.

Figure S17 compares the 2D ^{11}B-^{1}H correlation spectra acquired with different CP contact times, which are plotted with the skyline projections of ^{1}H and single-pulse ^{1}H MAS spectra displayed in vertical (left) axis and skyline projection of ^{11}B MAS NMR spectra plotted and single-pulse 1D ^{11}B MAS spectra plotted on the horizontal (top) axis in (a). It is noteworthy that the ^{11}B peaks at 6 and 10.2 ppm correspond to the boron atoms in *mono*- and *bis*-chelate complexes exhibit the correlation peaks with the ^{1}H signals in the range of 1.7-7.5 ppm, indicating the through-space proximities between the boron sites and the proton sites in the NMDG groups, and the polymer backbone.

19. 1D ^{11}B NMR spectra of boron adsorbed pristine and washed resin

Figure S18 presents the ^{11}B MAS spectra of boron adsorbed Amberlite IRA743 powder acquired before and after washing with Millipore water for three times. Peaks associated with the borate salts (agglomerates), chelate complexes and unreacted boric acid are labeled in (a). A significant reduction in the ^{11}B peak intensity corresponding to *mono*-chelate complexes is observed, which hence proves the lability of this species. Washing is also accompanied by the removal of free boric acid and borate anions as evidenced by reduced intensity of these peaks in (b).

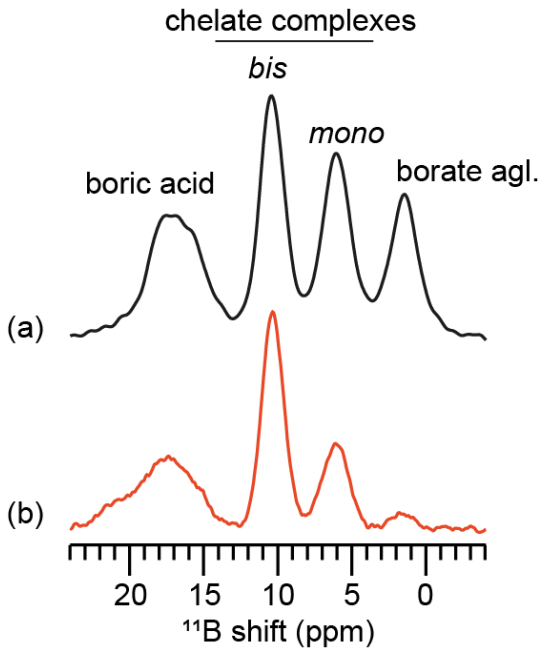

Figure S18. (a) ^{11}B NMR spectrum of boron-treated polymeric resin Amberlite IRA743 acquired before (top) and after (bottom) washing with Millipore water. All spectra were acquired at 18.8 T and 50 kHz MAS frequency**.** The boric acid concentration was 33.8 g/L.

20. References

(1) He, S.; Liu, C.; Chi, X.; Zhang, Y.; Yu, G.; Wang, H.; Li, B.; Peng, H. Bio-Inspired Lightweight Pulp Foams with Improved Mechanical Property and Flame Retardancy via Borate Cross-Linking. *Chem. Eng. J.* **2019**, *371*, 34–42.

(2) Wicklein, B.; Kocjan, D.; Carosio, F.; Camino, G.; Bergström, L. Tuning the Nanocellulose-Borate Interaction to Achieve Highly Flame Retardant Hybrid Materials. *Chem. Mater.* **2016**, *28*, 1985–1989.

(3) Fang, F.; Zhang, X.; Meng, Y.; Ding, X.; Bao, C.; Li, S.; Zhang, H.; Tian, X. Boron-Containing Intumescent Multilayer Nanocoating for Extinguishing Flame on Cotton Fabric. *Cellulose* **2016**, *23*, 2161–2172.

(4) Han, J.; Yue, Y.; Wu, Q.; Huang, C.; Pan, H.; Zhan, X.; Mei, C.; Xu, X. Effects of Nanocellulose on the Structure and Properties of Poly(Vinyl Alcohol)-Borax Hybrid Foams. *Cellulose* **2017**, *24*, 4433–4448.